Synthesized Emulsifiers from Kraft Lignin and the Role of Mixing in Oil-in-Water Emulsions

By

Mohammad Emamian

B.Sc. Chemical Engineering
University of Tehran, Tehran, Iran, 2021

Supervisors:

Dr. Leila Pakzad

Dr. Pedram Fatehi

A thesis submitted to the Faculty of Graduate Studies in partial fulfillment of the requirements for the degree of Master of Applied Science
in
Chemical Engineering

Summer 2023
Lakehead University
Thunder Bay, Ontario, Canada

Abstract

Synthesized Emulsifiers from Kraft Lignin and the Role of Mixing in Oil-in-Water Emulsions

Mohammad Emamian
MASc, Chemical Engineering, Lakehead University, Thunder Bay, 2023

Oil-in-water emulsions are widely used in various industrial applications such as food, pharmaceuticals, and cosmetics. An oil-in-water emulsion is a colloidal system in which oil droplets are dispersed in water with the help of emulsifiers. The emulsifiers can stabilize the oil droplets in the water phase, preventing them from coalescing and being separated from the water, resulting in a stable mixture that can be used in various industrial processes. Lignin macromolecules, derived from renewable biomass resources, have gained extensive interest during the past decade as a sustainable substitute for oil-based synthetic materials. One of the goals of this dissertation was to formulate and develop a lignin-based emulsifier that is renewable, biodegradable, and non-toxic from the molecular level to the macroscopic level. To obtain the desired physicochemical properties, chemical modifications were conducted. We utilized solvent-free reactions to synthesize sulfo-alkylated lignin-based emulsifiers in a facile green process. Oil-in-water emulsions were formulated in the presence of emulsifiers, and a vertical scan analyzer was used to monitor their stability to show their potential for stabilizing emulsions.

Additionally, this study examines the mixing process in oil-in-water. Mixing two immiscible liquids is an important part of achieving a stable emulsion, impacting product quality. One of the major factors affecting the stability of liquid-liquid dispersion is the droplet size distribution (DSD) of the dispersed phase. To enable real-time monitoring, we effectively employed the smart online

particle analysis technology (SOPAT) probe to measure the droplet sizes and DSD in an un-baffled stirred tank and an oscillatory baffled reactor (OBR) using dilute oil-in-water mixtures. Our investigation focused on impeller rotation speed, type, and the stirred tank's oil-water ratio. We observed that increasing the impeller speed led to a decrease in the Sauter mean diameter and resulted in DSDs shifting toward smaller droplet sizes.

Furthermore, use of a radial impeller promoted the formation of more uniform droplets and smaller droplet sizes. We also found that the dispersed phase volume fraction had a negligible effect on DSD in diluted liquid-liquid dispersions. We also examined the impacts of the baffle's oscillation amplitude and frequency of the OBR on droplet size and size distribution. Our experimental findings revealed that the oscillation amplitude and frequency had similar effects, effectively controlling droplet size and size distribution. Increasing either the amplitude or frequency resulted in a decrease in droplet size and a narrower distribution.

Acknowledgement

This study was conducted at Lakehead University in the Chemical Engineering department.

I would like to extend my heartfelt gratitude to my supervisors, Dr. Leila Pakzad and Dr. Pedram Fatehi, for their support, guidance, and access to this study's necessary testing facilities.

I would also like to express my appreciation to my thesis committee members, Dr. Francisco Ramos-Pallares and Dr. Kang Kang from the Department of Chemical Engineering, for their valuable insights and the time they dedicated to my research.

I am deeply thankful to Dr. Weijue Gao, Dr. Ayyoub Salaghi, Dr. Jonathan Diaz-Baca, Dr. Shrikanta Sutradhar, and all the members of the multi-phase research group and green processes research center for providing a warm and collaborative atmosphere throughout the past two years.

I also thank the Natural Sciences and Engineering Research Council of Canada (NSERC) for their financial support throughout this research. Furthermore, I would like to acknowledge the invaluable support of SOPAT GmbH during the entire duration of this study.

To my Parents, **Hamideh** and **Ahmad**,

Every day, I count my blessings for being in a world with parents like you, who radiate love and care. Your unwavering support has brought me to where I stand today.

Table of Contents

List of Tables

List of Figures

Introduction

Emulsions are known for their wide applications in cosmetic, paint, textile, and food industries (Goodarzi et al., 2019), consist of two immiscible liquids. Emulsifiers are essential to stabilize these systems, as emulsions without them are thermodynamically unstable (Wu et al., 2016). However, the current emulsifiers, derived from petroleum-based chemicals, are environmentally unfriendly, costly, and sometimes ineffective.

Researchers have explored biobased emulsifiers to overcome these challenges as alternatives for stable oil-water emulsions. Despite significant progress, there is still room for developing impactful bio-emulsifiers for various industries.

Lignin, the most abundant aromatic biopolymer on Earth, comprises 20 to 40% of the dry mass of wood (McDonald et al., 2001). Historically, lignin was considered an obstacle in papermaking due to its dark color and negative impact on paper strength. Delignification, necessary for producing paper from lignocellulose, generates substantial amounts of byproduct annually (Fatehi et al., 2016). In the 19th century, burning lignin as fuel was the solution. In the 1930s, sulfite pulping became the dominant method of producing wood pulp, resulting in lignosulfonates as a water-soluble by-product (Bajpai et al., 2018). Lignosulfonates (LS) found applications as dispersants, emulsion stabilizers, binders, and sequestrants (Macfarlane et al., 2014). However, the limited worldwide production of LS, accounting for only approximately 2% of the total chemical pulp production, posed drawbacks for its utilization (Österberg et al, 2020). To address this, the valorization of kraft lignin, traditionally viewed as low-quality, gained attention as an abundant raw material with the potential to replace fossil-based chemicals and products (Zakzeski et al.,

2010). Thus, lignin is expected to play a crucial role in the Canadian bioeconomy (Awasthi et al., 2020).

For effective lignin valorization, understanding its physicochemical structure is vital. Lignin comprises polyphenolic material derived from the enzyme-mediated polymerization of three phenylpropanoid monomers (Gharehkhani et al., 2019). However, lignin's structure and properties can vary based on its origin, plant type, and isolation methods (Ghaffar and Fan, 2013; Chakar et al., 2004). The first step is to determine suitable modification routes for lignin, quantifying its functional groups, internal linkages, molecular weight, and other physicochemical properties that influence modification processes. Various modification pathways such as polymerization, catalytic reactions, depolymerization, oxidation, and grafting have been explored, leading to unique properties in lignin (Upton and Kasko, 2016; Li et al., 2015; Sun et al., 2018; Gillet et al., 2017; Kazzaz, 2019).

Additionally, the formation of droplets and their significant role in creating a homogeneous and stable emulsion have garnered considerable interest. The droplet size distribution within these dispersions is a crucial aspect of design and scale-up. The stability of a mixture of two immiscible liquids and their interactions depends heavily on both hydrodynamics and droplet size distribution within the system's geometry. Maaß et al. (2012) introduced the smart on-line particle analysis technique (SOPAT) probe to measure droplet size. This equipment employs an endoscopic probe inserted into the two-phase mixing system, combined with a pulse laser, to capture image information of the insertion area. The automatic image analysis software then identifies and counts the droplets. Recently, researchers have shown increasing interest in measuring droplet size distribution using the SOPAT probe (Hohl et al., 2018; Panckow et al., 2017; Panckow, 2015).

Despite these studies, further investigations are needed to use the SOPAT for droplet size distribution measurement in liquid-liquid dispersions' mixing.

In chapters two, three, and four of this thesis, the first part (Known as "**Emulsifier Synthesizing**") explores the synthesis of emulsifiers derived from lignin, explicitly focusing on their physiochemical properties. The emphasis lies in understanding how these properties impact the stability of emulsions, and the second part (Known as "**Mixing**") introduces a novel approach involving a SOPAT probe to analyze how experimental conditions in different mixing systems influence droplet size and distribution, offering a fresh perspective on emulsion studies.

Chapter 2. ***Literature review*****:** In the first part of this chapter, the relevant topics to the subjects of oil-water emulsions and their applications, the use of bio-emulsifiers, and the production and use of lignin and lignin derivatives are reviewed, and the second part provides a literature review on mixing and its application in industry. The studies related to the droplet size and distribution, their measuring techniques, and the application of SOPAT in liquid-liquid dispersion are presented in this chapter.

Chapter 3. ***Experimental Design and Procedure*****:** In the first part of this chapter, the materials and experimental methodologies for generating and characterizing sulfoalkylated lignin polymers, their pH responsivity, zeta potential, contact angle, and the rheology and stability of oil-water emulsions are comprehensively explained. The second part of this chapter concerns the design, specification, and operation of the SOPAT probe. The experimental procedure and conditions are also provided in this chapter.

Chapter 4. ***Results and Discussions*****:** The initial section of this chapter demonstrates the characterization findings concerning synthesized sulfoalkylated lignin. It also discusses the impact of pH on the stability and rheology of emulsions stabilized by sulfonated lignin and the influence

of charge density and temperature on the stability and rheology of emulsions stabilized by sulfomethylated lignin. In the subsequent part, the successful application of the SOPAT probe is presented, which investigates the effects of various parameters, such as impeller speed, impeller type, oil-water volume ratio, and oil viscosity in a stirred tank, and frequency and amplitude in OBR, on droplet size and droplet size distribution.

Chapter 5. ***Overall Conclusions and Recommendation*****:** In this chapter, the overall conclusions of this thesis work are summarized, and future work to continue this research is suggested.

Finally, the relevant references cited in this thesis has been presented.

1.2 Research Objectives

As per the literature review presented in the following chapter, this study's initial phase focuses on synthesizing lignin-based emulsifiers through sulfoalkylated modification. It aims to investigate how characteristics such as charge density and pH impact the stability of oil-water emulsions. The second part of the study aims to explore the effects of various mixing parameters, including impeller speed, impeller type, fluid viscosity, and oil-water volume ratio in a stirred tank, as well as oscillation frequency and oscillation amplitude in OBR on Sauter mean diameter and droplet size distribution. The investigation has been carried out using the SOPAT probe to analyze droplet size distribution. It's worth noting that the complete evaluation of the SOPAT probe's application in mixing two immiscible liquids is still pending and requires further examination.

Literature Review

2.1 Emulsifier Synthesis

2.1.1 Emulsions

An emulsion is described as the dispersion of one liquid in another immiscible liquid, resulting in droplets of the dispersed phase suspended in the continuous phase. The continuous phase is referred to as the external phase, while the droplet-forming phase is known as the internal or dispersed phase of the emulsion. In the case of oil emulsions, crude oil typically constitutes one liquid phase, while the other is an aqueous phase or water. Emulsions can be categorized based on the droplet size in the continuous phase flow (Tarasov et al., 2018). When the dispersed droplets are larger than 0.1 mm, the emulsion is called a macro emulsion. The uniformity of dispersions can be affected by two standard destabilization processes: particle migration and variation or accumulation of droplet size. The stability of emulsions is subject to various phenomena, including coalescence, flocculation, sedimentation, phase inversion, creaming, and Ostwald ripening which is the growth of one emulsion droplet at the expense of a smaller one as a result of the difference in chemical potential of the material within the droplets (Fingas and Fieldhouse, 2004). Although many emulsifiers have been used to produce stable emulsions, the current emulsifiers are predominantly synthetic and expensive materials with significant environmental impacts. There have been efforts to develop environmentally friendly emulsifiers to reduce reliance on such synthetic materials. For instance, lignin-derived emulsion systems have been recently explored (Zembyla et al., 2020). However, the understanding of the effects of lignin-derived emulsifiers is still limited.

2.1.2 Emulsion Formulation

Two essential factors for the formation of emulsions when combining oil and water phases are adequate mixing and including a surface-active agent. In emulsion formulations, mixing is crucial in achieving a uniform distribution of oil and water within the systems. Generally, higher shear levels during mixing result in smaller droplet sizes of the dispersed phase, leading to a more stable emulsion (Zembyla et al., 2011). However, it's important to note that mixing and energy consumption are interconnected, and the mixing process may not always be favourable in emulsion systems. The second significant factor contributing to emulsion formation is the presence of an emulsifying agent. The type and stability of the emulsion are significantly influenced by the composition and quantity of the emulsifier used.

2.1.3 Types of Emulsions

Emulsions can be classified into two main groups: water-in-oil (W/O) and oil-in-water (O/W) emulsions (Goodarzi and Zendehboudi, 2019). In water-in-oil emulsions, water droplets are dispersed within an oil-continuous phase. In contrast, in oil-in-water emulsions, oil phase droplets are distributed within a continuous phase of water (Gellerstedt and Gustafsson, 1987). The specific type of emulsion formed depends on various factors, such as the water-to-oil ratio and temperature. Additionally, emulsions can be categorized based on the size of droplets in the continuous phase. Emulsions with dispersed droplets larger than 0.1 mm are referred to as macro-emulsions. These emulsions are generally thermodynamically unstable because the two phases tend to coalesce and separate over time due to a reduction in interfacial energies. However, stabilization mechanisms can counteract droplet coalescence rates (Tambe and Sharma, 1995). In contrast, the second category of emulsions, known as micro-emulsions, forms when two immiscible fluids coexist due

to their extremely low interfacial energy. The droplet size in micro-emulsions is less than 10 nm, making them thermodynamically stable mixtures. Micro-emulsions exhibit significant differences from macro-emulsions in terms of their stability and formation processes (Healy et al., 1987)

2.1.4 Characteristics of Emulsions

To achieve a stable emulsion, emulsifiers play a crucial role in altering the interfacial properties, thereby preventing coalescence events (Maphosa and Jideani ,2018). Another prerequisite for stable emulsion formation is maintaining sufficiently small droplet sizes, enabling collision forces on continuous phase molecules to induce Brownian motion, preventing settling (Tadros, 2013). Notably, freshly prepared emulsions may exhibit distinct features from aged ones due to variations in oil type caused by absorbable components, differences in emulsifier adsorption rates, and their capacity to form an interface film. Significant alterations in temperature or pressure can lead to notable changes in emulsion characteristics, including viscosity and droplet size (Ghosh and Rousseau, 2010). Emulsifying agents are designed to stabilize emulsions and can be categorized into two types: finely divided solids and surface-active agents (Binks et al., 1999). Fine solids generally provide mechanical stabilization to emulsions. These materials, wetted by both water and oil, should be smaller than emulsion droplets and accumulate at the water/oil interface. The efficacy of these particles in stabilizing emulsions is heavily influenced by such factors as inter-particle interactions, particle size, and material wettability. Fine solid constituents present in the produced oil may include clay particles, sand, asphaltene/wax, silt, and mineral scales deposited at the water/oil interface (McLean and Kilpatrick ,1997; Urbina-Villalba ,2009). Surface-active agents or surfactants are particles soluble in both oil and water phases. They possess a hydrophilic branch that interacts with oil and a hydrophobic branch with an affinity for water. Surfactants tend

to form an interfacial film at the oil-water interface (Schramm et al., 2003), thereby reducing interfacial tension (IFT) and consequently enhancing droplet dispersion and emulsification.

2.1.5 Mechanism of Emulsifiers

From a thermodynamic standpoint, an emulsion is inherently an unstable system due to the natural tendency of a liquid/liquid mixture to minimize its interfacial interactions and energies(Alinezhad et al., 2010). Oil-field emulsions are commonly classified based on their degree of kinetic stability. Emulsion stability primarily relies on the interactions between surface-active agents and water/oil interfaces. Following the initial formation of droplets, the emulsion changes over time due to several time-dependent processes, including Ostwald ripening, coalescence, flocculation, sedimentation, and creaming (Mohammed et al., 1994). The stabilization mechanisms of water-oil emulsions stem from their assumption as liquid/liquid colloidal dispersions. Their kinetic stability is achieved through small droplet sizes and the formation of an interfacial layer between the water and oil droplets. Emulsion stabilization is enhanced by the injection of emulsifiers, leading to electrostatic and steric forces. In the context of water-oil emulsions produced from oil fields, stabilization occurs through forming a thin film at the interface of the suspended droplets in the continuous phase. These films increase emulsion stability by enhancing the viscosity of the interfacial film (Raya et al., 2020). The viscous interfacial films slow down the drainage rate during water droplet coalescence by creating a repulsive barrier, consequently reducing the emulsion breakdown rate(Costa et al., 2019). The properties of interfacial films are influenced by several factors, including polar molecules, concentration in the heavy oil, type of crude oil (asphaltic and paraffinic), aging time, temperature, and pH, as well as the composition of the water phase (Bonto et al., 2019).

2.1.6 Application of Emulsions

The ability of emulsions to combine and stabilize disparate phases has led to innovative solutions in fields ranging from pharmaceuticals to food processing. This literature review highlights some critical applications of emulsions and their significance in contemporary research.

Food and Beverage Industry: Emulsions play a pivotal role in formulating a wide array of food products. For instance, in the production of mayonnaise, emulsifiers ensure the stable dispersion of oil droplets in an aqueous medium. Furthermore, emulsions are employed in creating creamy dressings, spreads, and dairy products, contributing to texture enhancement and flavor delivery (Tan and McClements, 2021).

Pharmaceuticals: The pharmaceutical sector capitalizes on emulsions for controlled drug delivery and improved bioavailability. With their small droplet size, nanoemulsions provide efficient solubilization of hydrophobic drugs and enhance absorption. Such formulations offer the potential for targeted therapies and improved therapeutic outcomes (Khan et al. 2011).

Cosmetics and Personal Care: Emulsions serve as the foundation for many cosmetic products, including lotions, creams, and sunscreens. The uniform distribution of active ingredients ensures optimal skin penetration, moisturization, and sun protection. Furthermore, emulsions provide a pleasing sensory experience to consumers (Venkataramani et al., 2020).

Enhanced Oil Recovery: Emulsions are harnessed in the oil industry for enhanced oil recovery techniques. Water-in-oil emulsions are injected into reservoirs to displace oil, reduce viscosity, and improve oil mobility. The stability of these emulsions aids in efficient oil extraction (Zhou et al., 2019).

Agriculture: Emulsions find application in the formulation of pesticides and herbicides. These formulations enhance the uniform distribution of active compounds, increasing their efficacy and reducing environmental impact. Emulsions offer a controlled release of agrochemicals, prolonging their effects (Chappat, 1994).

Environmental Remediation: In environmental cleanup efforts, emulsions are employed to encapsulate and transport hydrophobic pollutants. This strategy facilitates the removal of contaminants from soil and water systems, mitigating environmental hazards (Zha et al., 2017).

Emulsions, with their multifaceted applications, continue to inspire research in diverse domains. Innovations in emulsion formulation, stability enhancement, and tailored functionalities hold promise for addressing complex challenges across industries.

2.1.7 Surfactants

Surfactants play a vital role in the chemical industry, as they are utilized to modify various phases. They serve as emulsifiers, stabilizing liquid-liquid mixtures and dispersants for solid-liquid systems. These versatile applications make surfactants essential in producing foods, agrochemicals, pharmaceuticals, personal care products, and detergents in the industrial sector (Alwadani and Fatehi, 2018). Surfactants are characterized by a hydrophilic head and a hydrophobic tail, and they can be categorized into three main subgroups: anionic, cationic, and amphoteric surfactants (Schramm et al., 2003). Anionic surfactants form in the presence of carboxylates, sulfonates, sulfates, or phosphates. Among these, sulfonate-based anionic surfactants are widely used due to their broad solubility range and high tolerance against hydrolysis at varying pH levels, which makes them suitable for diverse industrial applications (Crepaldi et al., 2002). However, synthesizing sulfonate-based anionic surfactants is complex and expensive (Alwadani

and Fatehi, 2018). Leading to increasing demand for more environmentally friendly alternatives with simpler production processes. Polymeric surfactants have shown significant benefits over conventional small-molecule surfactants in recent decades. They possess unique characteristics, such as multiple functional groups, complex conformational changes at the oil interface, and the ability to enhance the viscosity of emulsions (Chang et al., 2015). Among polymeric surfactants, biobased materials have garnered substantial interest due to their biocompatibility, biodegradability, renewability, and long-term stability (Kalliola et al., 2018). Consequently, there is a growing need to develop novel bio-based polymers with surfactant properties (Alwadani and Fatehi, 2018).

2.1.8 Lignin Resources and Isolation

Lignin constitutes approximately 25-30% of plant cell walls, alongside cellulose and hemicellulose, making up the major polymeric components (Boerjan et al., 2003). Its primary role involves serving as a matrix material that binds the plant polysaccharide microfibrils and fibres, providing strength and rigidity to the plant stem. Additionally, owing to its chemical structure, lignin exhibits antioxidant and antimicrobial properties (Yang et al., 2018; Espinoza-Acosta et al., 2016). acting as a protective shield against biological attacks and assisting in water transportation by sealing plant cell walls to prevent water leaks (Ralph et al., 2004).

Technical lignin can be extracted through pulping chemical processes, which may involve sulfur or be sulfur-free. There are five distinct types of classified technical lignins, namely kraft, lignosulfonate, soda, organosolv, and hydrolysis lignin, each possessing unique physicochemical properties as summarized in **Table 2.1** (Kazzaz and Fatehi, 2020).

Table 2. 1. Chemical and physical properties of different commercial lignin. (Kazzaz and Fatehi, 2020)

Type	Sulfur content (wt.%)	Sugar content (wt.%)	Molecular weight (g/mol)	Ash content (wt.%)	Moisture content (wt.%)	Poly-dispersibility
Kraft	1-3	1-2.3	<25000	0.5-3	3-6	2.5-4
Lignosulfonate	3.5-8	-	<15000	4.5-8	5.8	4.2-9
Soda	0	1.5-3	<15000	0.7-2.3	2.5-5	2.5-3.5
Hydrolyzed lignin	0-1	10-22.4	5000-10000	1-3	4-9	1.5-3
Organosolv	0	1-3	<5000	1.7	7.5	1.5-2.4

This thesis focuses on kraft lignin, the most readily available type of technical lignin. In the kraft process, white liquor, a potent alkali solvent containing aqueous sodium hydroxide and sodium sulfide, breaks the bonds between lignin and cellulose. Consequently, the linkages among the phenylpropane units of lignin macromolecules are cleaved into smaller chains, rendering kraft lignin soluble in the pulping liquor system, and this soluble form is referred to as black liquor (Chakar and Ragauskas, 2004). In kraft pulp mills, black liquor is predominantly utilized as fuel for recovery, providing the mills with their energy requirements (Van Heiningen, 2006). Various isolation methods from black liquor have been developed to commercially produce technical kraft lignin, with LignoBoost™ and LignoForce™ technologies being standard processes (Rodrigues et al., 2018; Dessbesell et al., 2020). As depicted in Table 1, incorporating aliphatic thiol groups contributes to a high sulfur content (1 to 2 wt%) in kraft lignin, conferring hydrophobic properties (Kai et al., 2016).

2.1.9 Lignin Chemistry

Lignin's chemical structure is formed through an irregular radical oxidative coupling of three fundamental phenylpropane monomers: p-coumaryl alcohol, coniferyl alcohol, and sinapyl alcohol, collectively known as "monolignols". These monolignols give rise to heterogeneous repeating alcoholic units, leading to the formation of p-hydroxyphenyl (H), guaiacyl (G), and syringyl (S) polymerized products, as depicted in **Fig. 2.1** (Sun, 2010). As a result of the polymerization of these monomers, various wood species and specific parts of trees, such as softwoods, hardwoods, and non-woods, can exhibit notable chemical distinctions with unique molecular structures (Ralph et al., 2004). In softwoods, lignins primarily comprise guaiacyl (G) units, along with minimal quantities of hydroxyphenyl (H) and syringyl (S) components (Sun, R. ,2010). On the other hand, hardwood lignins consist of both guaiacyl (G) and syringyl (S) lignins, accompanied by small amounts of hydroxyphenyl (H) lignin. Non-wood lignins typically include all three precursors - guaiacyl (G), syringyl (S), and para-hydroxyphenyl (H) - in varying ratios (Derkacheva and Sukhov, 2008). These variations in lignin composition contribute to its diverse properties and make it a versatile material found in different plant tissues. Understanding these chemical differences is crucial for various industrial applications involving lignin, such as biofuel production, pulp and paper manufacturing, and biorefinery processes (Ralph et al., 2004).

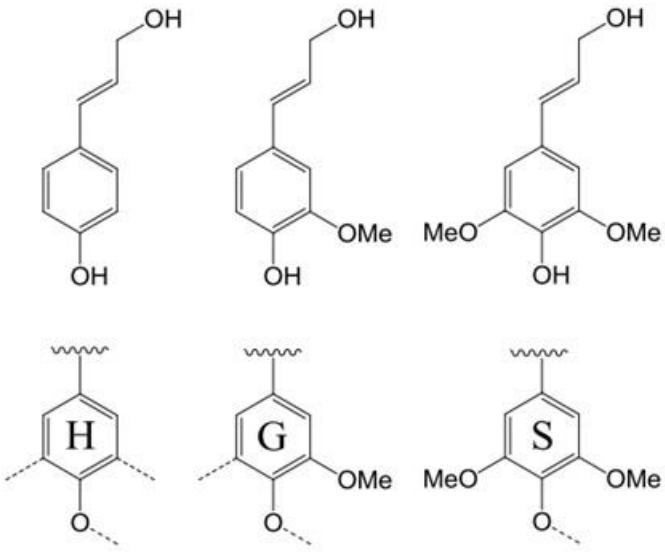

Fig. 2.1. Lignin precursors including monolignols p-coumaryl alcohol, coniferyl alcohol, and sinapyl alcohol (top row) and the corresponding p-hydroxyphenyl (H), guaiacyl (G), and syringyl (S) units of lignin

2.1.10 Value-added Products from Lignin

Numerous researchers have recognized the abundant benefits of lignin, including its ready availability, high energy density (kJ/g), active chemical structure, and sustainability. This has sparked interest in enhancing lignin's compatibility and applicability across various industries. A notable objective has been developing lignin-based products that can replace petroleum-derived materials, promoting green and sustainable alternatives (Zakzeski et al., 2010). Over the past few decades, lignin has been utilized for different applications through three main strategies. The first approach involves using lignin without or with minimal modification, allowing for specific applications that align with its inherent properties. However, further modifications are required in most cases to unlock lignin's potential in diverse applications. Another strategy involves the degradation of lignin into smaller chemical compounds, like vanillin, which researchers have

extensively explored have extensively explored. Subsequent chemical changes to the degraded lignin, such as (1) reducing its molecular weight, (2) minimizing steric hindrance, (3) increasing reactive sites, and (4) enhancing phenolic hydroxyl content, have been advantageous for synthesizing lignin-phenol-formaldehyde resins (Laurichesse et al., 2014; Mathias and Rodrigues, 1995; Mathias and Rodrigues, 1995; Kalami et al., 2018). The third category involves tailoring lignin's properties through chemical modification of its active sites to produce polymers with varying characteristics, including hydrophobic or hydrophilic nature, different molecular weights, charge densities, wettability, and surface and interfacial properties (Laurichesse et al., 2014). Polymers sourced from natural materials hold immense promise for creating innovative and cutting-edge applications. The following section explore a prevalent method of producing lignin polymers through chemical modification. This technique has been pursued to harness the potential of lignin and develop advanced materials suitable for various applications.

2.1.11 Graft Functionalization

Numerous techniques for graft functionalization of lignin have been documented in the past decade. This approach has gained popularity due to its straightforward chemical process, effectiveness, high degree of grafting, and the resulting solubility of the final polymers. Functionalization can occur on the phenolic, aliphatic hydroxyl groups, or directly on the ring structure. Some examples of these methods include oxidation (Gharehkhani et al., 2018) oxyalkylation (Kühnel et al., 2018), halogenation (Sequeiros et al., 2016), amination (Zheng et al., 2017), carboxy alkylation (Bahrpaima and Fatehi, 2018). and sulfoalkylation (Konduri and Fatehi, 2015). These functionalized polymers, characterized by their solubility, adjustable charge density, and molecular weight, have found application in various fields, such as dispersants (Zhang et al., 2018), flocculants (Tian et al., 2014), binders (Chen et al., 2020), thickeners (Cortés-Triviño et al.,

2018), emulsifiers, and detergents (Chen et al., 2016). This thesis is focused on a simple and facile process to produce sulfonated and sulfomethylated lignin as a lignin-based emulsifier.

2.1.12 Applications of Lignin

Applications of lignin-derived polymers have been extensively explored, leading to a diverse range of materials with varied properties (Gharehkhani et al., 2018; Kühnel et al., 2018; Sequeiros et al., 2016; Zheng et al., 2017; Ghavidel and Fatehi, 2018; Bahrpaima and Fatehi, 2018; Konduri and Fatehi, 2015; Zhang et al., 2018; Tian et al., 2014; Chen et al., 2020; Cortés-Triviño et al., 2018; Chen et al., 2016). The suitability of each polymer for specific applications depends on the modifications made to lignin, resulting in distinct characteristics. For instance, polymers formed by polymerizing lignin and acrylic acid, exhibiting high molecular weight and charge density, have shown promise as potential flocculants for wastewater treatment (Kong et al., 2015; Ataie et al., 2020). On the other hand, a high molecular weight polymer lacking surface charges and solubility, like lignin-styrene-divinylbenzene, can serve effectively as an adsorbent (Podkościelna et al., 2015). Low molecular weight polymers with high charge density have proven to be suitable dispersants for coal slurry (Konduri et al., 2015), while those with lower charge density can act as ideal emulsifiers, adsorbing at the oil interface to function as polymeric surfactants. Consequently, such polymers hold potential as environmentally-friendly alternatives to oil-based additives in various applications.

2.2 Mixing

2.2.1 Introduction to Mixing

The science of mixing describes the development of the concentration content in various substances, and it refers to any process used to convert a non-uniform system into a uniform one (i.e., the random distribution of two or more previously separated phases). Blending, dissolving, dispersion, suspension, emulsification, heat transfer, and chemical reactions are all chemical or physical processes that require mixing (Zhang et al., 2012). It is widely utilized in the chemical, petroleum, pharmaceutical, and food sectors, among others (Tang et al., 2020). This is the process of combining two or more immiscible liquids, solids and liquids, or liquids and gases. "Blending" has been defined as mixing miscible liquids, whereas "mixing" has been defined as dispersing immiscible liquids or producing emulsions.

Mixing is classified into three levels based on the length scale: macro-mixing, meso-mixing and micro-mixing. Macro-mixing refers to attaining homogeneity at the reactor scale. Meso-mixing refers to the coarse-scale turbulent exchange between the fresh feed and its surrounding. Micro-mixing refers to the viscous-convective deformation and the molecular diffusion process (Duan et al., 2020). Due to its vast application, mixing has attracted much attention, and several studies have been conducted to investigate this process.

2.2.2 Classification of Mixing Based on Phases

2.2.2.1 Gas-Liquid Mixing

Many processes in the chemical industries, such as oxidation, hydrogenation, wastewater treatment, and biological are carried out in the gas-liquid agitated vessels (Heidari, 2020). The

primary aims of gas-liquid mixing include evenly distributing the gas phase in the liquid phase, optimizing the total interface area between two phases, and enhancing the overall rate of mass or heat transfer and chemical reaction in industrial operations (Gu et al., 2021). In these processes, the gas phase is distributed as bubbles in the liquid phase using the mixing technique to boost the mass transfer rate between the phases and improve process efficiency. Another essential element in gas-liquid mixing is bubble size, which is crucial in factors such as heat transfer. One of the most significant characteristics in evaluating product quality and processing cost is the performance of the gas-liquid two-phase mixing.

2.2.2.2 Solid- Liquid Mixing

Another type of mixing is solid-liquid mixing, which has various applications and has been the subject of many studies in the literature. The impact of solid-liquid mixing is a striking factor in the production, transport and homogenization operations inherent to the pharmaceutical, mining, chemical, food processing and cosmetics industries. Poor mixing can be responsible for large operating costs for these industries due to poor yield, over-consumption of energy and product fouling (Blais et al., 2016). For instance, stirred tanks are used as reactors for crystallization and catalytic reactions and play a key role in the homogenization of products and the dissolution of solids in the pharmaceutical, cosmetic and food industries (Blais et al., 2017). Turbulently agitated vessels where a solid-liquid suspension is produced account for approximately 80% of all industries and are common in leaching process, crystallization process, catalytic reactions, bio-slurry processes, mineral processing, precipitation, coagulations, dissolution, water treatment, and a variety of other applications. Solid-liquid mixing in mechanically agitated vessels is a widely used process in a multitude of industries, including ore processing, pharmaceuticals and cosmetics (Blais and Bertrand, 2017; Raja Ehsan Shah et al., 2015). These processes are primarily performed

in stirred tank units, specially designed to ensure a high contact area between the phases and avoid solid build-up at the bottom of the tank (Rossi et al., 2022). In the process of mixing solids and liquids, it's crucial to understand how the solid particles are spread throughout the stirred tank. This information is a key factor for effectively increasing the scale of the process and achieving the best possible mixing results (Ibrahim et al., 2019).

2.2.2.3 Liquid- Liquid Mixing

Between the mixing of different components, the mixing of two or more liquids has attracted particular attention. The components may be miscible liquids or immiscible liquids.

- **Miscible Liquids Mixing**

The miscible liquids are said to be perfectly and effectively mixed when the mixing is done at the molecular level. In general, there are two types of processes when it comes to the mixing in miscible liquids. One is mixing within the same solvent, and the other is mixing in different solvents (Wang et al., 2012) . Mixing of different liquids confined within a small volume is an important issue in many emerging technologies, such as lab-on-a-chip, semiconductor cleaning, and polymer processing (Kim et al., 2015). Also, it is essential. in particular in a range of applications exemplified by droplet-based coating methods. Recently, limited work studied the CFD of the mixing of liquid-liquid miscible flow, the blending of liquids of different density and viscosity in a static mixer, the mixing of water-ethanol in the T-shape microdevice, the mixing behavior of ethanol and glycerol in the stirred tank equipped with an anchor impeller using the Modified Algebraic Slip Mixture (MASM) multiphase model under laminar flow, the homogenization of miscible liquid with different densities in a flat bottom cylindrical stirred tank equipped with a pitch blade turbine using the Lattice-Boltzmann method (LBM) without the use

of modelling turbulence (Madhania et al., 2017). Disturbances in the interfaces of miscible liquids are known to grow to instability due to an unfavorable pressure gradient arising from a density difference in the gravity field resulting in "density fingering", or due to the viscosity difference in a flow in confined (porous) geometries resulting in "viscous fingering" (Has and Sunthar, 2021).

- **Partially Miscible Liquids Mixing**

Some liquids are partially miscible. Two liquids are considered partially miscible if there is a set of compositions over which the liquids will form a two-phase liquid system. This is a common situation and is the general case for a pair of liquids where one is polar and the other non-polar (such as water and vegetable oil). Understanding the flow dynamics of multiphase systems with partially miscible components is relevant to many industrial applications, such as the extraction and purification of chemicals (Ghaemi et al., 2021). Some examples of partially miscible liquids are glycerol/water and soybean oil/hexane binary mixtures, which are miscible in any proportions (Xie and Vorobev, 2016).

- **Immiscible Liquids Mixing**

The other type of liquid-liquid system is immiscible liquid mixing, which is of special importance in many industrial and biological applications. In mixing immiscible liquids, the minor component is generally present as the dispersed phase (drops or filaments) in a continuous phase of the major component (Anderson and Meijer, 2009). The immiscible liquid-liquid dispersion system is widely used in chemical, petroleum, pharmaceutical, polymerization, food, and other industries.

2.2.3 Mixing Systems

Depending on the different desired drop sizing, the power requirements and the process conduction (batch or continuous), various equipment options are at hand, such as baffled and unbaffled stirred

tanks, static mixers, rotor-stator mixers, impingement mixers, and ultrasonic mixers. Mixing operations are usually conducted by stirred tanks when droplet size distribution (DSD) from micrometre to millimetre scale is desirable (Len and Calabrese, 2003). Another type of mixer is an oscillatory baffled reactor (OBR), a particular type of tubular reactor, typically equipped with periodically located sharp-edged orifice baffles along its length. The OBR operates with a periodic oscillatory (or pulsed) flow. The pulsed flow interacts with the baffles and causes effective transverse flows and enhanced transport. Avila et al. (2022) reviewed oscillatory baffled reactors (OBRs) design, performance characterization, and applications. Lobry et al. (2015) studied continuous suspension polymerization transposition, predominantlyliquid–liquid dispersion step. The oscillatory baffled reactor was employed to investigate the mentioned processes. It became clear from the outputs that using this type of mixer makes it possible to produce controlled droplet size distribution and droplet breakage is mainly dominated by oscillation.

2.2.4 Droplet Size Distribution

The drop size distribution is a crucial property in particulate processes and is affected by many quantities and factors. Experimental drop size measurement in immiscible liquid dispersion systems has still been challenging. Several liquid-liquid dispersion studies have focused on DSD and studied both experimentally and numerically (Canu et al., 2018; Perlekar et al., 2012; Liu et al., 2006; Floury et al., 2000) Oil type, which takes the oil density, viscosity, and oil-water interfacial tension into account significantly impact droplet size distribution. Researchers with different industrial goals have studied the effect of oil type on DSD (Hole et al., 2019; Maindarkar et al., 2015; Taherian et al., 2006). The dispersed phase volume fraction is a significant parameter for the mixing process and plays an essential role in the stability of the emulsion. An increase in the dispersed phase can increase the interfacial area, enhancing the mass and heat transfer

(Mollakhalili Meybodi et al., 2014; Tcholakova et al., 2011; Sengupta et al., 2006). The mixer's function and DSD depend on many parameters, such as impeller type (shape) and the number of baffles. Therefore, understanding how these parameters influence the performance of mixers will significantly contribute to optimizing the implementation of this set of equipment and reaching the appropriate DSD. In the literature, a few studies have systematically compared the drop size distribution produced by different designs of impellers. Several experimental studies in liquid-liquid dispersion have focused on the Rushton turbine (O'Rourke and MacLoughli, 2005; Quadros and Baptista, 2003; Pacek et al.,1999). Zhou and Kresta (1998) studied the drop size in a highly dilute liquid-liquid system with a Rushton turbine and three axial flow impellers. At the same time, they did not compare the impellers. The number of impeller blades significantly impacts the DSD, which Giapos et al. (2005) showed by decreasing the blade number from 8 to 2, a 52% increase in mean droplet size was observed. The other factor affecting the DSD is impeller speed, which is particularly interesting in getting suitable DSD (Wade et al., 2014; El-Hamou et al., 2009; Lovick et al., 2005).

2.2.5 Droplet Size Measurement Techniques

One commonly employed and straightforward method for measuring droplet size involves the sample withdrawal approach. The dimensions of the collected droplets were subsequently evaluated through microscopy (Godfrey and Grilc, 1977; Kumar et al., 1991)or photometry (Verhoff et al., 1977). Limitations of this method encompass a biased selection of specific droplet sizes and its applicability restricted to dilute dispersion systems, as noted by Godfrey and Grilc (1977) Solsvik and Jakobsen (2015) employed a high-speed imaging method to analyze the fracture mechanism within a liquid-liquid dispersion system. Nonetheless, this technique's drawback is the potential inadequacy of the sample image in representing all the available droplet

sizes in the dispersion system. Recent advancements in laser technology, including laser diffraction and laser backscattering methods, have introduced novel approaches to particle size measurement that address the short-comings above. Utilizing an optical reflectance measurement (ORM) particle size analyzer and an endoscope, Lovick et al. (2005) obtained real-time droplet size distributions (DSD) for a kerosene-in-water dispersion system encompassing a volume fraction range of 10-60%. Their findings indicated that the impact of the dispersed phase's volume fraction on droplet size is negligible in highly concentrated dispersions. Li et al. (2017) explored the influence of a non-ionic surfactant (specifically, Tween 80) concentration on the DSD of oil-in-water dispersion within a stirred tank, both experimentally and numerically. They concluded that elevating surfactant concentration led to a reduction in the mean droplet size and an enhancement in emulsion stability. Zhou and Kresta (1998) harnessed the phase Doppler particle analyzer (PDPA) to measure droplet size, velocity, and concentration. They comprehensively reviewed available measurement techniques and correlations about droplet size in liquid-liquid dispersions. Boxal et al. (2010) established a correlation between droplet size measurements using two distinct particle size assessment methods: particle video microscopy (PVM) and focused beam reflectance measurement (FBRM). Wang et al. (2013) employed the FBRM technique to monitor the evolution of droplet size during the mixing of oil-in-water dispersions, focusing on phase inversion across volume fractions ranging from 10% to 60%.

2.2.6 Smart Online Particle Analysis Technique (SOPAT)

Maaß et al. (2012) initially developed a smart online particle analysis technique (SOPAT) probe to measure the droplet size. In this equipment, an endoscopic probe is inserted into the two-phase mixing system, combined with the pulse laser, to obtain image information of the insertion area. The automatic image analysis software performs the identification and count of droplets. The

measurement of droplet size distribution through the SOPAT probe has attracted the attention of researchers in recent years (Hohl et al., 2018; Panckow, 2017; Panckow, 2015). Tang et al. (2020) used SOPAT to measure the droplet size distribution and mean droplet size in liquid-liquid dispersions in a rectangular mixer with a pump impeller. They observed that the mean droplet size decreased by increasing impeller speed or decreasing dispersed phase holdup. Röhl et al. (2019) experimentally studied the impact of different silica nanoparticles on rheology, interfacial tension, and drop size distributions in liquid-liquid systems. In their investigation, conducted in a stirred tank, a SOPAT probe was used to measure the droplet size distribution. They took advantage of two different endoscopes with the transfixion principle with a measurement range of particle diameters between 8-600 μm and 25-1000 μm.

Experimental design and procedure

3.1 Emulsifier Synthesis

3.1.1 Materials

Softwood kraft lignin (KL) obtained through the LignoForceTM technology was received from FPInnovations. Chemicals, including sodium sulfite (Na_2SO_3), formaldehyde (CH_2O 37 wt.%), polydimethyldiallyl ammonium chloride (PDADMAC 100,000–200,000 g/mol), para-hydroxybenzoic acid (0.5%), potassium hydroxide (KOH, 0.8N), sodium hydroxide (NaOH, 97%), sodium nitrate ($NaNO_3$), sulfuric acid (H_2SO_4, 98%), hydrochloric acid (HCl, 37%), trimethylsilylpropanoic acid (TSP, 99.8%), and dimethylesulphoxide-d6 (DMSO-d_6) were purchased from Sigma-Aldrich (Canada) and used without any further purification. Spectrum Labs provided dialysis membrane with a cutoff of 1,000 g/mol. Deionized water with a resistivity of less than 18 MΩ-cm was generated using a Millipore water purification system and utilized for all experiments conducted in this study. The olive oil utilized in this research was also obtained from a nearby supermarket.

3.1.2 Lignin Sulfoalkylation

In previous investigations, various routes for sulfo-functionalization were explored using kraft lignin, with the examination of different reaction parameters, including time, temperature, and molar ratio (Gao et al., 2019; Konduri and Fatehi, 2015). Based on the insights gained from these systematic studies, appropriate reaction conditions were selected for the current study's sulfo-functionalization of the KL sample.

3.1.3 Sulfonation

For this series of reactions, 0.5 g of KL sample was dispersed in water in a three-neck flask equipped with a magnetic stirrer to achieve a 15 g/L lignin concentration. Subsequently, Na_2SO_3 powder was added to the mixture in a molar ratio 1/1. The pH of the reaction medium was adjusted to approximately 11 using a 1M NaOH solution, after which the mixture was heated in a water bath at 90 ℃ for 3 hours. The solution was then cooled to room temperature, neutralized with 5% $H2SO_4$(aq), and subjected to membrane dialysis for two days, with water changes every 2 hours during the first 6 hours and then once daily for the next two days to facilitate purification. The sulfonated kraft lignin sample was obtained by evaporating the water from the solutions at 60 ℃ in an oven.

3.1.4 Sulfomethylation

The sulfomethylation of the KL sample was carried out following a previously described method. A 40 g/L lignin solution was prepared in a three-neck flask, and formaldehyde (37 wt.%) was added at different formaldehyde-to-lignin molar ratios of 0.5/1, 1/, and 3/1. The pH of the solution was adjusted to approximately 11 using a 2.5 mol/L NaOH solution, and the mixture was heated Na_2SO_3-to-lignin molar ratio of added formaldehyde, and the reaction was allowed to proceed for another 3 hours at 90 ℃. Upon completion of the reaction, the purification and drying steps were carried out as described in the previous section.

3.1.5 ^{1}H–NMR Analysis

The ^{1}H-NMR spectra of the kraft lignin, sulfonated lignin, and sulfomethylated lignin were recorded using a Bruker AVANCE Neo NMR-500 MHz instrument (Switzerland) and Topspin 4.02 version software. For analysis, 70 mg of the samples were dissolved in 1 mL of DMSO-d6

that contained 2 mg of TSP at 50 ℃ and shaken in a water bath shaker overnight at 50 rpm. Afterward, 1 mL of each solution was transferred into the NMR tube for analysis. Sixty-four scans were recorded, and the pulse width was 90° in the NMR analysis.

3.1.6 Solubility Determination

To determine the solubility of lignin samples, 0.2 g of unmodified lignin or modified lignin was added to 20 ml of deionized water. The mixture was stirred at 100 rpm for 2 hours at 30 °C using a water bath shaker. After the stirring period, the samples were centrifugated at 1000 rpm for 5 minutes, and the resulting supernatant was dried overnight in a 60 °C oven. It is important to note that lignin obtained through the LignoForce technology exhibits diverse structures and molecular weights, which can impact its solubility characteristics (Kouisni et al., 2012). Due to these variations, the modification process may not entirely solubilize all lignin segments. To address this, the solubility of lignin in the supernatant was expressed as weight percent (wt.%) to directly quantify the extent to which the original lignin segments were solubilized. The calculation of the solubility of lignin in the supernatant was determined using the provided **Equation (3.1)**.

$$\text{Water Solubility (wt.\%)} = \frac{\text{Mass of dissolved lignin}}{\text{Initial mass of lignin}} \times 100 \quad \textbf{(3.1)}$$

3.1.7 Charge Density

To measure the charge density of lignin samples, modified lignin was first dried at 105 °C overnight to eliminate any residual moisture. Subsequently, a 0.2 g portion of the lignin samples was dissolved in 20 ml of deionized water and incubated for 1 hour at 30 °C in a water bath shaker set at 150 rpm. After the incubation period, the samples were centrifugated at 1000 rpm for 10 minutes, and the resulting supernatants were collected for charge density analysis using a particle

charge detector (Mutek, PCD 04, Germany). The charge density was determined by titrating the supernatants against a PDADMAC standard solution (0.005 M).

3.1.8 Elemental Analysis

The elemental analysis of lignin samples was conducted using an Elementar Vario EL Cube elemental analyzer through a combustion analysis method. The samples were dried overnight at 105 °C to eliminate any moisture. About 2 mg of unmodified and modified lignin samples were precisely weighed and placed in silver vessels, which were then loaded into the integrated carousel of the elemental analyzer. Subsequently, the samples were automatically transferred into a combustion tube and subjected to combustion at a high temperature of 1200 °C. The combustion gases resulting from this process were then reduced and analyzed to determine the carbon, hydrogen, nitrogen, and sulfur content of the lignin samples. This analysis aimed to provide valuable information about the elemental composition of the lignin samples (Jahan et al., 2012).

3.1.9 Molecular Weight Analysis

The molecular weight of modified lignin was evaluated using gel permeation chromatography (GPC), Malvern Viscotek GPCmax, (Malvern, UK), with a UV detector. In this set of experiments, 4 mg/mL sample solutions were prepared by dissolving dried powders of modified lignin in 10 mL of 0.1 mol/L $NaNO_3$ solutions. After filtration with a 0.2 μm nylon filter (13 mm diameter), the samples were passed through PolyAnalytic, PAA206, and PAA203 columns at 35 °C at the flow rate of 0.70 mL/min. At the same time, polyethylene oxides were used as standard polymers for calibration.

3.1.10 Phenolic Group Analyses

The phenolic group of unmodified and modified lignin polymers was measured using an automatic potentiometric titrator (785 DMP Titrino, Metrohm, Switzerland). About 0.06 g of dried lignin polymers were added to 100 mL of deionized water containing 1 mL of 0.8 mol/L potassium hydroxide in a 250 mL beaker. After stirring at 200 rpm for 5 min, 4 mL of 0.5 % parahydroxybenzoic acid solution was added as an internal standard, and the solution was titrated with 0.1 mol/L hydrochloric acid solution. During the titration, with the decrease in the pH of the sample solutions, three endpoints appeared in sequence (v_1', v_2', and v_3', respectively). The corresponding three endpoints in the titration curve of the blank sample (i.e., sample without lignin) were quantified as v_1, v_2, and v_3, respectively. The phenolic hydroxyl contents of samples were calculated according to **Equation (3.2)** [1].

$$\text{Phenolic hydroxyl group } \left(\frac{\text{mmol}}{\text{g}}\right) = \frac{C_{HCl}\,[(v_2'-v_1')-(v_2-v_1)]}{m} \quad \textbf{(3.2)}$$

where C_{HCl} is the concentration of HCl solution (0.1 mmol/L) as the titrant, and m is the mass (g) of the sample. v_1, v_2, and v_3 are the volumes (mL) of HCl solution consumed for the three endpoints in blank titration. v_1', v_2', and v_3' are the volumes (mL) of HCl solution consumed for the three endpoints in sample titration, respectively. Results are the average of three repetitions.

3.1.11 Zeta Potential

The zeta potential of the sulfonated lignin solution was determined using a NanoBrook PALS (Brookhaven Inc., USA). Sulfonated lignin solutions at a concentration (1 wt.%) with different pH were prepared by using 0.1 M of HCl or 0.1 M of KOH to adjust the pH via stirring at 300 rpm and 25°C overnight. Afterward, 250 µL of potassium chloride was added to 1 L MiliQ water and

stirred for 30 min. Then, 20 mL of KCl solution was filtrated and used in this measurement. Afterward, 1 mL of sulfonated lignin solutions was added to 20 mL of the filtrated KCl and sonicated for 15 seconds. The zeta potential analysis was executed at room temperature and a constant electric field of 8.4 V/cm. The reported data was the average of three repetitions.

3.1.12 Contact Angle Measurement

For the contact angle measurement, the two-phase water contact angle (WCA) was determined using a theta optical tensiometer attention (Biolin Scientific). First, 300 µL of sulfomethylated lignin solutions at concentrations of (1 wt.%) were coated on clean glass slides. The coated films were dried in the oven at 105°C overnight. Then, a drop of deionized water (5 µL) was placed on the coated glass slides, and the contact angle of samples at the water-air interface (WCA) was determined following static contact angle (i.e., two-phase contact angle) measurement via the sessile drop method at 25 °C for 10 sec. The contact angle of sulfomethylated lignin on a glass slide coated with oil was measured using the following method: First, the glass slide was soaked in oil, and then excess oil was removed from one side of the slide. Next, a 5 µL drop of sulfomethylated lignin solution was placed on the oil-covered glass slide. The contact angle was then determined like measuring the water-air interface contact angle (WCA).

3.1.13 Emulsion Preparation

Stock aqueous solutions of modified lignin solutions (0.25 wt.%) at pH 3, 7, and 11 were prepared. The volumetric ratio of unity of aqueous modified lignin solution and olive oil, as the organic phase, was prepared in clean glass vials and emulsified using an ultrasonic machine (Omni-Ruptor 4000, Omni International Int.) at room temperature, 240 W power and 60 s for 3 s intervals.

3.1.14 Stability Analysis

The stability of the emulsion systems was studied using a vertical scan analyzer for 24 h. The samples were prepared inside the glass container of the instrument and subjected to analysis. The sample was scanned with a pulsed near-infrared light (λ = 880 nm), and the transmitted and backscattered lights were recorded by the instrument's detectors, in which a microscopic fingerprint of the samples could be recorded. The stability of samples was quantitively analyzed in terms of stability index (TSI), where both coalescence and settling phenomena are considered in TSI evaluation. The TSI is determined by **Equation (3.3).**

$$TSI = \sqrt{\frac{\sum_{i-1}^{n}(x_i - x_{bs})^2}{n-1}} \quad \textbf{(3.3)}$$

where n, x_i, x_{bs}, refer to the number of scanning, the average of the backscattered light intensity at the scanning time, and the average of x_i, respectively. The higher the TSI, the lower the stability is (Gharehkhani et al. 2018).

3.1.15 Rheology Properties

A hybrid rheometer (TA Instruments) with a parallel plate geometry (8 mm, gap 300 μm) was used to perform the rheological studies of formulated emulsions at room temperature. About 1 mL of each sample was carefully taken by pipet and placed on the lower plate of the instrument. A 3 min pre-shear at 100 s^{-1} was applied on each sample before starting the measurements. Viscosity variations were measured from 0.1 to 1000 s^{-1} at 23 °C. An amplitude sweep was performed in the range of 0.01 and 100 s-1 at frequency of 10 rad/s to determine the linear viscoelastic region. Frequency sweep measurements were then carried out in the 0.01 and 100 rad/s range with a strain of 0.1% chosen from the linear viscoelastic region.

3.2 Mixing

3.2.1 Stirred Tank

The first part of the experiments was conducted in a cylindrical tank with a flat bottom. The tank had a height of 250 mm (H_T) and an inner diameter of 220 mm (D_T), and the liquid inside reached a height of 145 mm (H_l), as demonstrated in **Fig. 3.1**. The tank could accommodate various types of impellers, including axial. radial. and axial-radial. all positioned 72.5 mm (H_I) above the tank bottom. A SOPAT probe (SOPAT GmbH) was also present, situated at the same height as the impellers, near the tank wall, connected to a computer and controlled by SOPAT software. To drive the impellers, a 0.2 hp direct-driven motor was utilized. **Fig. 3.2** provides a schematic representation of the impellers and their dimensions.

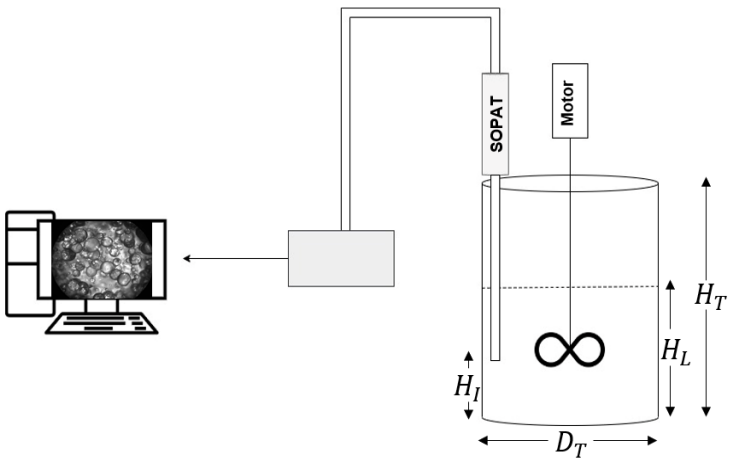

Fig. 3.1. The schematic of the stirred tank setup

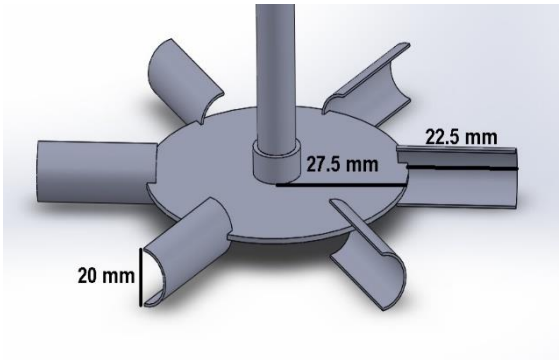

Radial impeller (Scaba)

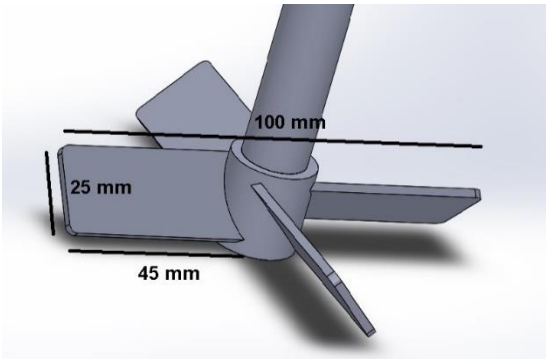

Axial impeller (A200)

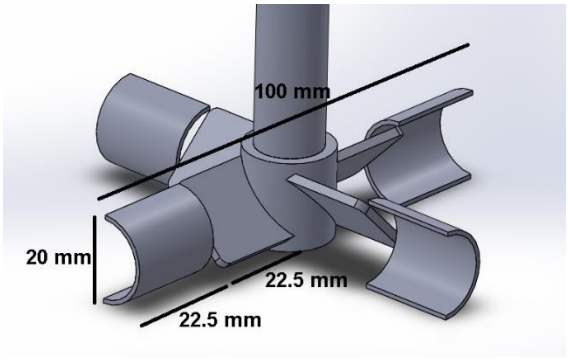

Axial-radial impeller (ASI)

Fig. 3.2. The schematic of impellers and their dimensions

3.2.2 OBR

The second part of the experiments focused on the OBR. A DN4O OBR system (NiTech Solutions Ltd) with a working volume of 230 ml was utilized. The OBR apparatus consisted of a reactor vessel equipped with baffles. A SOPAT probe was placed inside the OBR vessel to facilitate real-time monitoring and droplet size measurements. The SOPAT probe was connected to a computer

running SOPAT software, allowing for data acquisition and analysis. The reactor setup, probe, and connection to the computer and SOPAT software are presented in Fig. 3.3. This setup is located in the multiphase flow research (MFR) laboratory, CASES Building, Lakehead university.

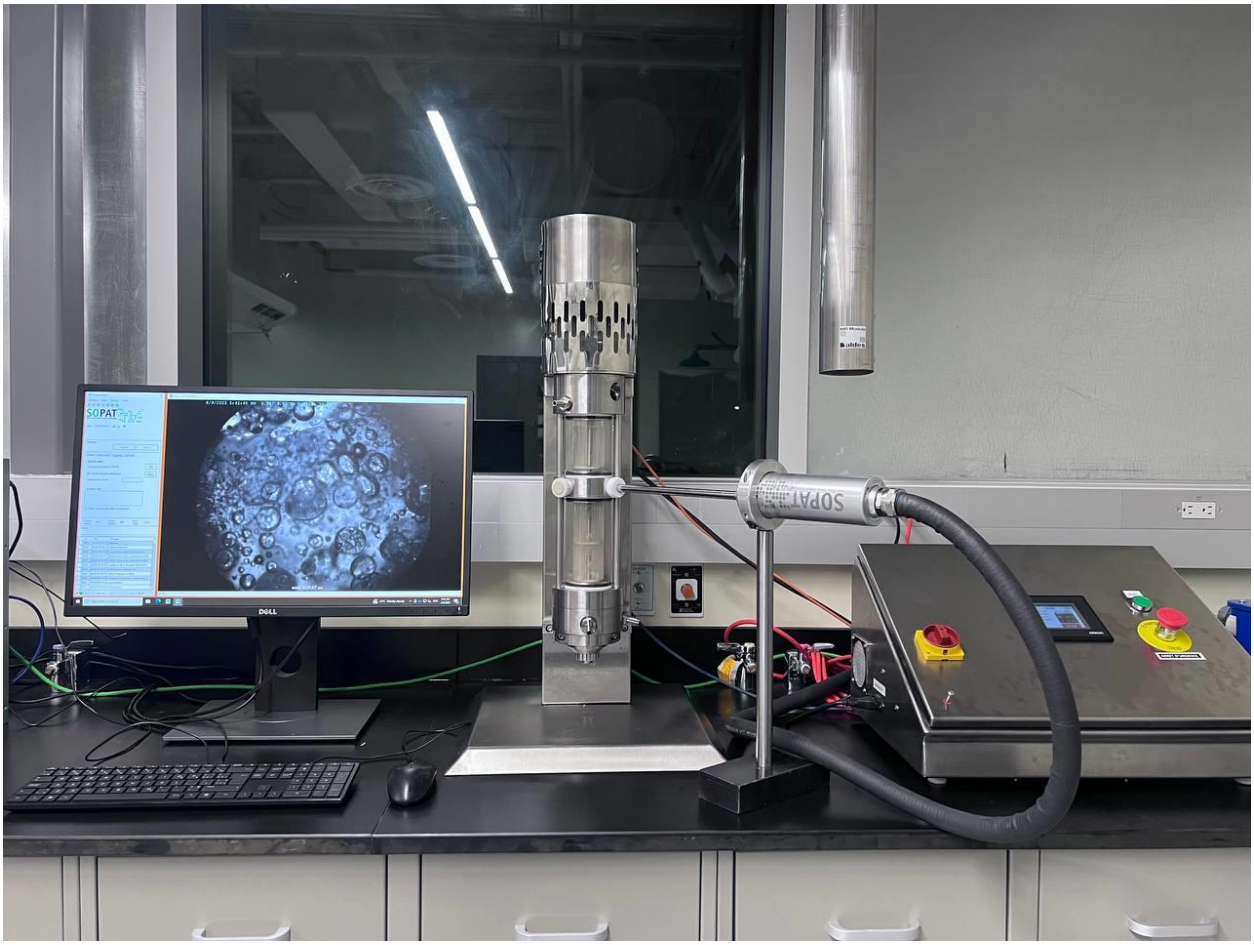

Fig. 3.3. The schematic of the OBR setup

3.2.3 Material Properties

Two different oils, canola and olive oils, were used as dispersed phases and tap water as a continuous phase. The physical properties of the materials are presented in **Table 3.1**.

Table 3.1. Physical properties of fluids at 22 °C and 1 atm (Sahasrabudhe et al., 2017)

Fluid	Density (kg/m^3)	Viscosity (mPa.s)	Interfacial Tension (mN/m)
Water	1,000	1.0	-
Canola oil	913	63.5	31.30
Olive oil	908	74.0	31.90

3.2.4 Experimental condition

- Stirred Tank

The effect of impeller speed, impeller type, volume fraction of oil, and oil type was evaluated in this study. The experimental conditions are summarized in **Table 3.2**. The Reynolds number was determined within the span of 1000 to 4000 for these conditions. The chosen variable ranges were carefully selected for scientific and engineering purposes:

Impeller speed: 150 rpm as a baseline, 200 rpm for moderate mixing, and 250 rpm for intense agitation investigation, ensuring diverse conditions. These selections ensured various conditions, maintaining liquid containment within the tank while providing sufficient energy to disrupt droplets without spillage. The volume fraction of oil: 2.5% for low-concentration understanding, 5.0% for moderate impact, and 10.0% for high-concentration insights. Oil type: canola and olive oils for their distinct properties. Impeller type: Radial, radial-axial, and axial for varied flow

patterns and mixing efficiency analysis, offering a comprehensive understanding of impeller design impact.

Table 3.2. Experimental conditions for stirred tank

Experimental variables	**Range**
Impeller speed	150, 200, and 250 rpm
Volume fraction of oil	2.5%, 5.0%, and 10.0%
Oil type	Canola and olive oil
Impeller type	Radial, radial-axial, and axial

- OBR

The effect of oscillation amplitude and oscillation frequency were evaluated in this study. The experimental conditions are summarized in **Table 3.** The oscillatory Reynolds number was determined within the span of 1000 to 8000 for these conditions. The chosen range of oscillation frequency and amplitude in the OBR experiments was determined by the need to provide sufficient energy for breaking oil droplets while accounting for the limitations of the DN4O OBR syst. Additionally, the placement of the SOPAT probe within the OBR restricted the ability to use higher oscillation amplitudes.

Table 3.3. Experimental conditions for OBR

Experimental variables	**Range**
Oscillation amplitude	9, 18, and 27 mm
Oscillation frequency	1, 2, and 3 Hz

Volume fraction of oil	2.5%
Oil type	Canola

3.2.5 Experimental Procedure

Before each test, both the mixing tank and OBR were cleaned. They were then filled with the desired volume of oil and water for each case according to **Tables 3.2** and **3.3**. Fresh oil and water samples were used for every test. The systems were left undisturbed for a few hours to reach room temperature, and mixing started. The DSDs were measured after one hour of mixing (to ensure a stable system). This time frame was determined based on preliminary tests that tracked droplets over time. The DSDs were measured in situ using the SOPAT probe, an incident light endoscope measuring technique. The probe has a minimum detectable drop size of 15 μm. A Rhodium (Rh) mirror was positioned 6 mm from the endoscope tip to enhance image quality. Each measurement point involved capturing 30 images to ensure a minimum of 2,000 droplets were considered for each drop size distribution analysis. **Fig. 3.4** displays a representative example of the raw and analyzed images obtained from the SOPAT system.

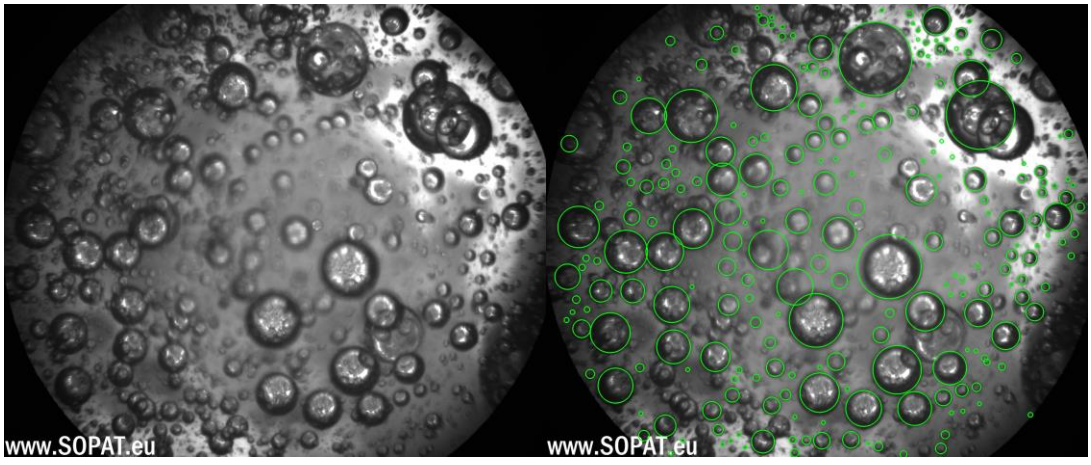

Fig. 3.4. Sample images of the raw and analyzed images obtained from the SOPAT system (Axial impeller, 250 rpm, $\varphi = 2.5\%$, canola oil)

3.2.6 Repeatability Tests

Repeatability tests for measuring the Sauter mean diameter were conducted under identical operational conditions on three days. The results are illustrated in **Fig. 3.5**, revealing an error range of 4 to 6% for each test. This error level signifies a strong reliability level for the experimental methods established within this study.

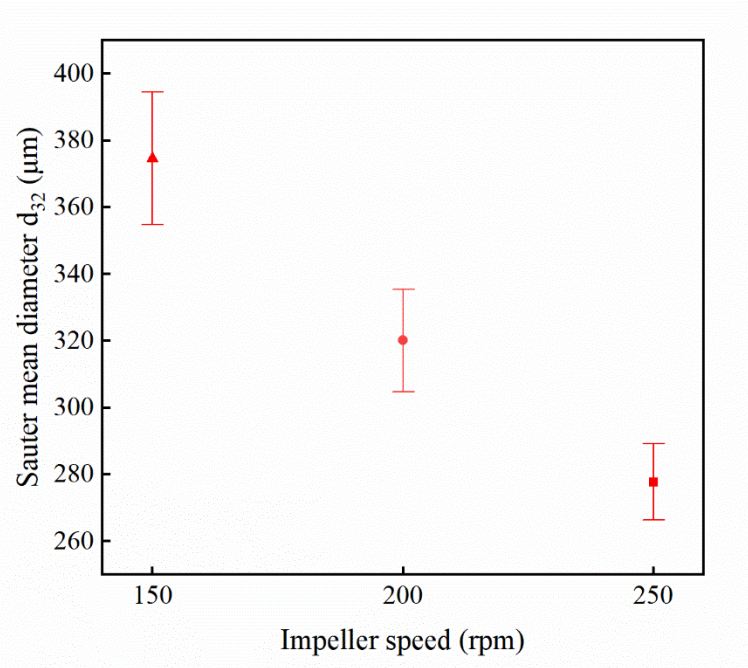

Fig. 3.5. Repeatability of Sauter mean diameter (Radial impeller, $\varphi = 2.5\%$, canola oil)

Results and Discussion

4.1 Emulsifier Synthesizing

4.1.1 Sulfonated Kraft Lignin Properties and ^{1}H–NMR Spectroscopy

Sulfonation involves replacing the aliphatic hydroxy groups of lignin with sulfonate groups, as depicted in **Fig. 4.1**, resulting in a negatively charged lignin molecule (Rojo et al., 2015). The primary site of this reaction is the α position carbon (Fengel and Wegener, 2011).

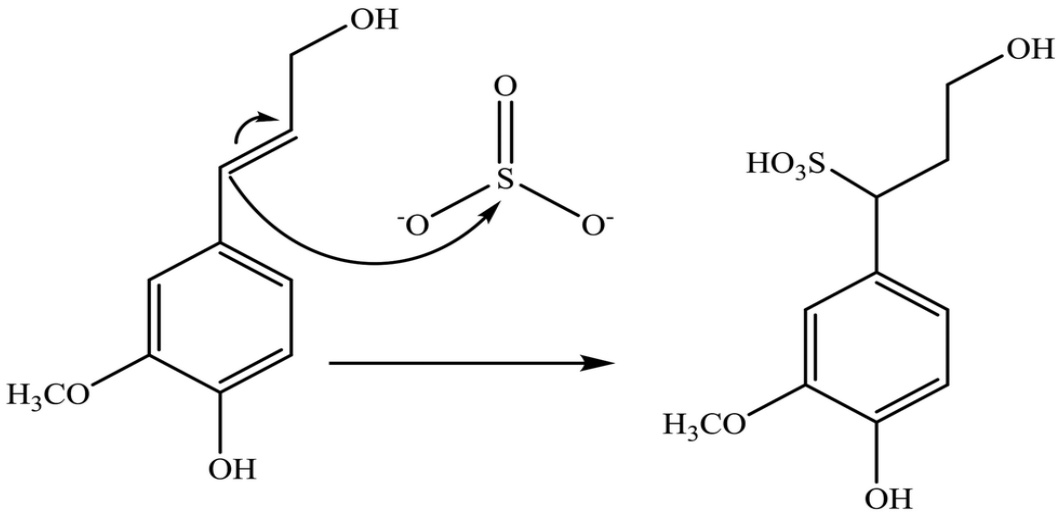

Fig. 4.1. Sulfonation of lignin with sodium sulfite

The structures of kraft lignin and sulfonated lignin were examined using ^{1}H-NMR spectra in DMSO-d6, shown in **Fig. 4.2**. In all the spectra, the peak at 2.58 ppm is from DMSO-d6. For kraft lignin, there are two broad peaks: 6.8–7.5 ppm is from the aromatic ring protons, and 3.2–3.8 ppm is from the methoxy groups (Bahrpaima and Fatehi, 2018). The significant rise in aliphatic proton signals of sulfonated lignin at 2.73 ppm can be attributed to the breaking of lignin, leading to the formation of a more complex carbon chain structure (Zhang et al., 2017).

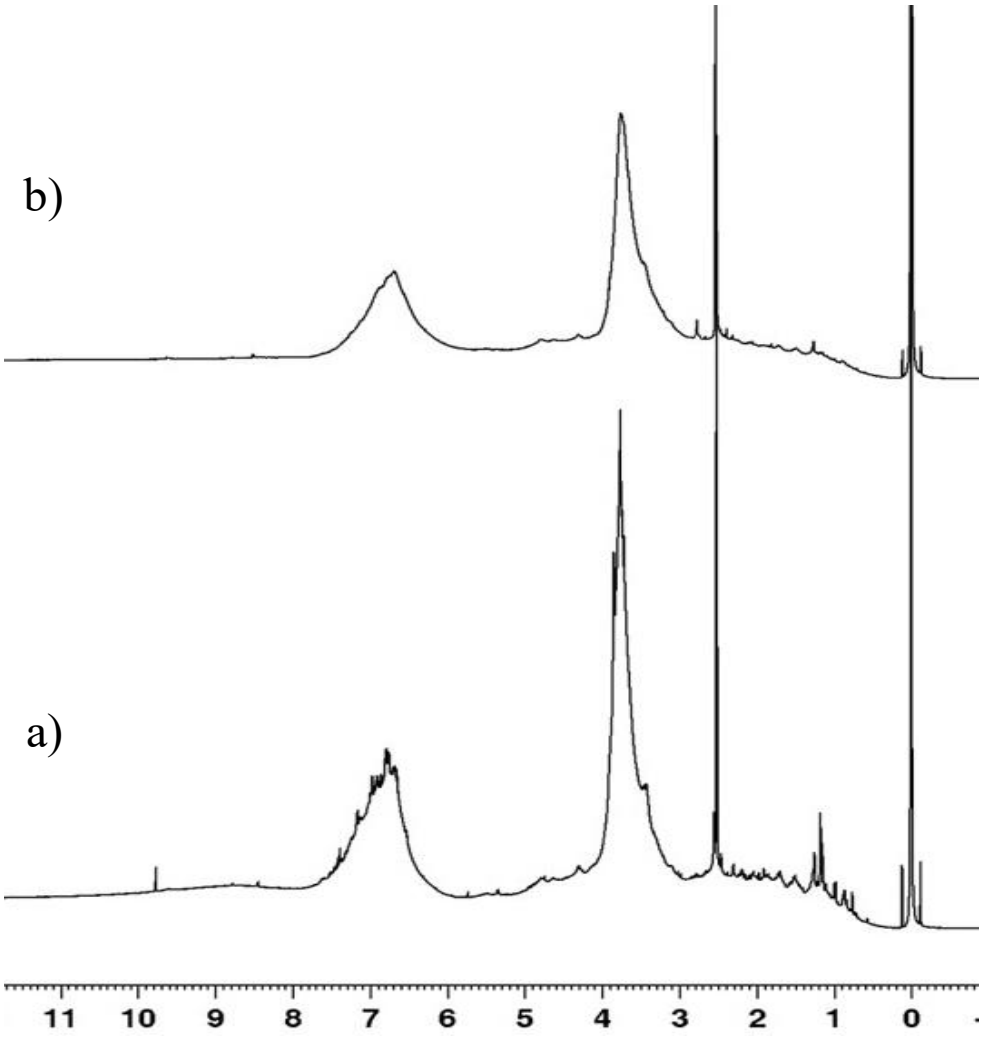

Fig. 4.2. ^{1}H–NMR Spectra of kraft lignin (a), and sulfonated lignin (b) in DMSO-d6

Table 4.1 presents an overview of the properties exhibited by softwood kraft lignin and sulfonated kraft lignin. The data indicates the successful synthesis of a water-soluble polymer with specific characteristics. Notably, the polymer demonstrates a charge density of 1.29 (meq/g), indicating the presence of charged groups within the molecule. This property makes the polymer suitable for

various applications that require charge-based interactions. Furthermore, the synthesized polymer exhibits a molecular weight of 2595 (g/mol), which provides insight into its size and mass distribution. This information determines its behavior and performance in different environments and applications. The molecular weight of the polymer indicates its potential for forming stable solutions, as higher molecular weights often contribute to improved solubility and reduced tendencies for precipitation or aggregation (Abdelghafour et al., 2021).

Table 4.1. Properties of softwood kraft lignin and Sulfonated kraft lignin

Sample	Charge density (meq/g)	Solubility %	C%	H%	N%	S%	Molecular weight (g/mol)	Phenolic group (mmol/g)
Softwood Kraft lignin	-	42	64.67	7.44	0.09	1.28	-	0.958
Sulfonated Kraft lignin	1.29	100	60.59	6.24	0	1.02	2595	0.496

4.1.1.1 Aggregation of Sulfonated Lignin

The samples' stability depends on the interactions between particles within the solutions, encompassing both repulsive and attractive forces. When there is a substantial repulsion between particles, it plays a crucial role in promoting particle stability. This repulsion between particles acts as a protective force, preventing their aggregation or precipitation, thereby contributing to the system's overall stability. In contrast, if the attractive forces between particles overpower the repulsive forces, it can lead to particle aggregation or instability within the solution. Therefore, understanding and manipulating the balance between repulsive and attractive forces is essential

for controlling the stability of the samples and ensuring their optimal performance in various applications (Ghavidel and Fateh, 2020). Sulfonated kraft lignin solution (0.25 wt.%) exhibited remarkable stability under neutral pH conditions for a prolonged time, as depicted in **Fig. 4.2.** Additionally, the system remained stable when the pH was adjusted to 11, creating an alkaline environment. However, altering the system's pH to a highly acidic level of 3 disrupted its stability, leading to the aggregation and formation of nano-sized sulfonated kraft lignin.

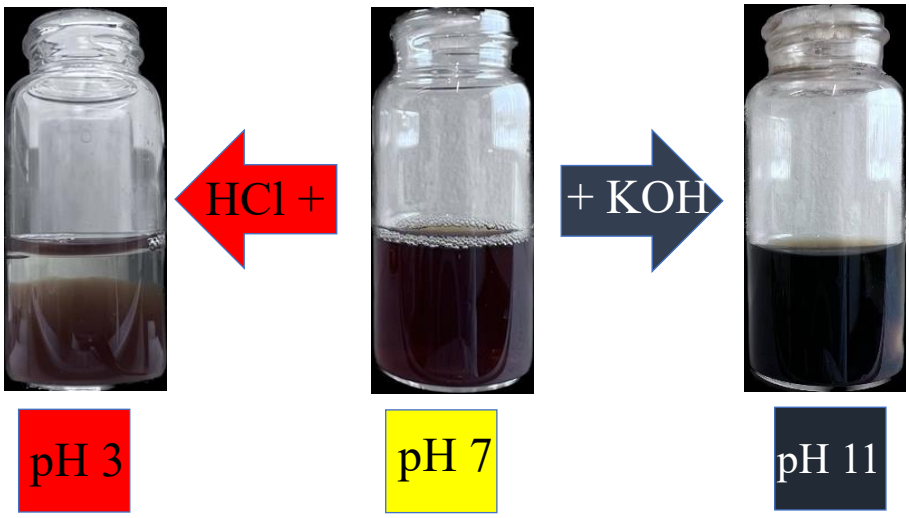

Fig. 4.3. Sulfonated kraft lignin solution (0.25 wt.%) at different pH

4.1.1.2 Zeta Potential

Fig. 4.3 presents quantitative measurements demonstrating a gradual and continuous increase in zeta potential (ζ) values as the pH decreases from 11 to 3. At pH 11, the zeta potential is recorded at -57 mV; at pH 3, it reduces to -25 mV. This observation highlights a notable influence of pH on the system's stability. The higher stability observed under neutral and alkaline conditions can be attributed to charged sulfonate groups within the polymer structure. These charged groups generate sufficient electrostatic repulsion among the polymer segments. As a result, the polymer chains

experience a repulsive force, preventing their proximity and subsequent aggregation or precipitation. The continuous increase in zeta potential with decreasing pH indicates a weakening of the electrostatic repulsion between the polymer segments. Consequently, the system's stability diminishes as the pH becomes more acidic. This phenomenon occurs due to the functional groups undergoing protonation (Ghavidel and Fatehi, 2020).

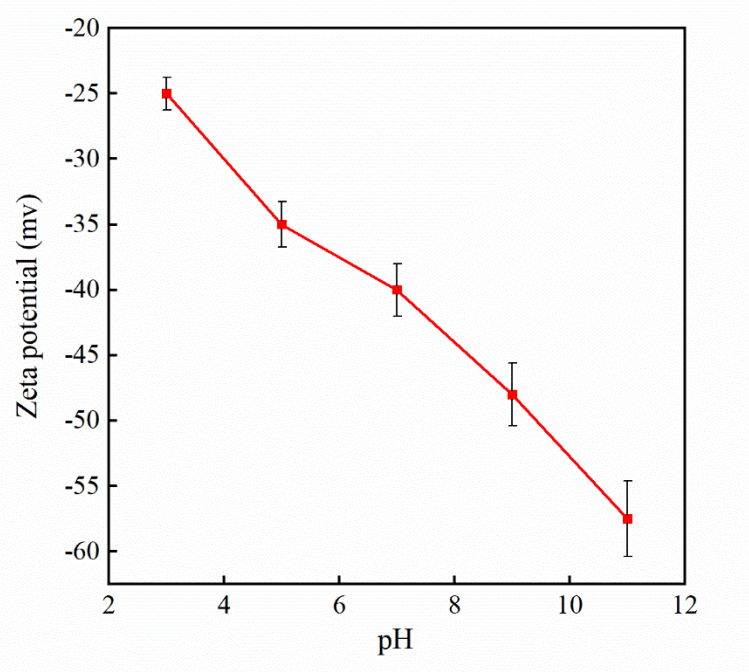

Fig. 4.4. Zeta potential (ζ) of sulfonated kraft lignin as a function of pH

4.1.1.3 Emulsion Stability Assessment

In this research, emulsions with different levels of stability were formulated using sulfonated kraft lignin at a dosage of 0.25 wt.%, depending on the pH conditions. As depicted in **Fig. 4.4**, it is evident that sulfonated kraft lignin polymers exhibit a migration toward the oil phase at pH 3 due to their heightened hydrophobicity. This increased hydrophobicity can be attributed to the protonation of their functional groups (Ghavidel and Fatehi P, 2020). Consequently, after 24 h, a

distinct separation is observed, with a clear water portion settling at the bottom of the vial. Notably, this phenomenon does not occur in the emulsions at pH 7 and 11, indicating a balance between the hydrophobic and hydrophilic properties of the sulfonated lignin polymer at these pH levels. As the pH increases, sulfonated kraft lignin demonstrates a greater inclination toward displaying its hydrophilic properties. This hydrophilicity contributes to a more effective stabilization of our emulsions. The pH-dependent behavior of the sulfonated lignin polymer highlights its dual nature, with the ability to exhibit both hydrophilic and hydrophobic characteristics. Understanding this balance is crucial for optimizing the stability and performance of emulsions in various applications (Zheng et al., 2023).

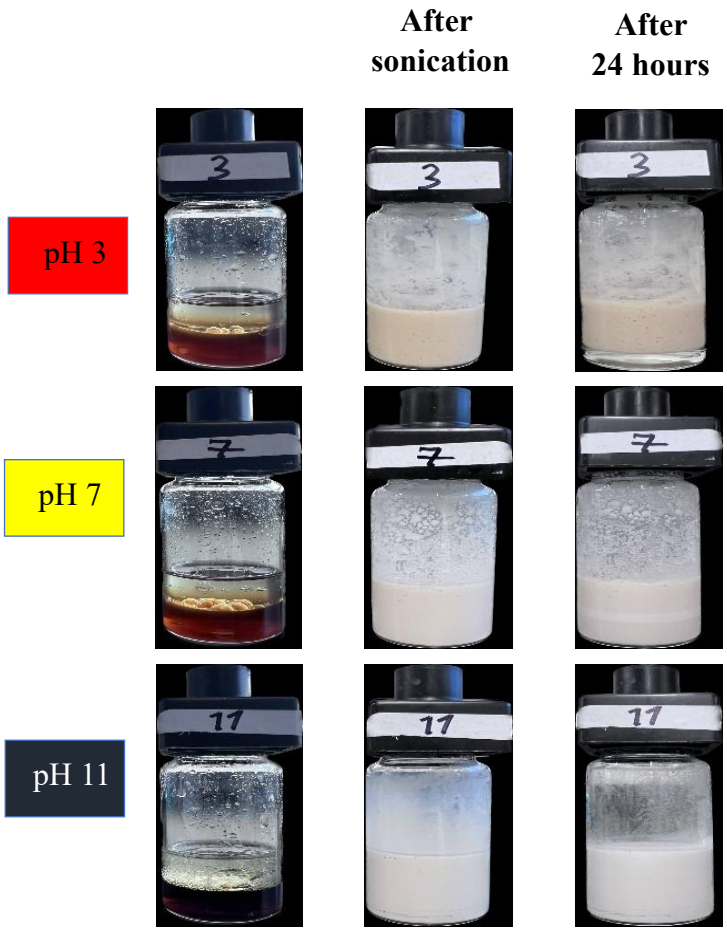

Fig. 4.5. The 24 h emulsion observation upon pH alteration

Fig. 4.5 illustrates the dynamic changes in the stability index values of the emulsion sample over a specific duration. In the case of the samples subjected to alkaline conditions (pH 11), the stability index (TSI) remained nearly constant after 24 h, indicating a high level of stability. This observation suggests that these samples maintained their emulsion structure without significant phase separation or destabilization over an extended time (Kowalska et al. 2020). Conversely, at pH 7, an evident phase separation occurred within the first two h following the emulsion's preparation. The separation process exhibited a nearly linear trend thereafter, suggesting a gradual and continuous separation of the oil and water phases. This behavior indicates lower stability compared to the alkaline conditions.

Interestingly, the sample at pH of 3 experienced a rapid phase separation, indicating diminished stability. This accelerated separation suggests a weaker interaction between the oil and water phases, leading to an early breakdown of the emulsion structure. These results collectively demonstrate that emulsion samples with higher pH values not only exhibit enhanced stability but also reach equilibrium conditions at a faster rate. The findings from **Fig. 4.5** provide valuable insights into the influence of pH on emulsion stability, highlighting the importance of pH control in optimizing emulsion systems' performance and shelf life.

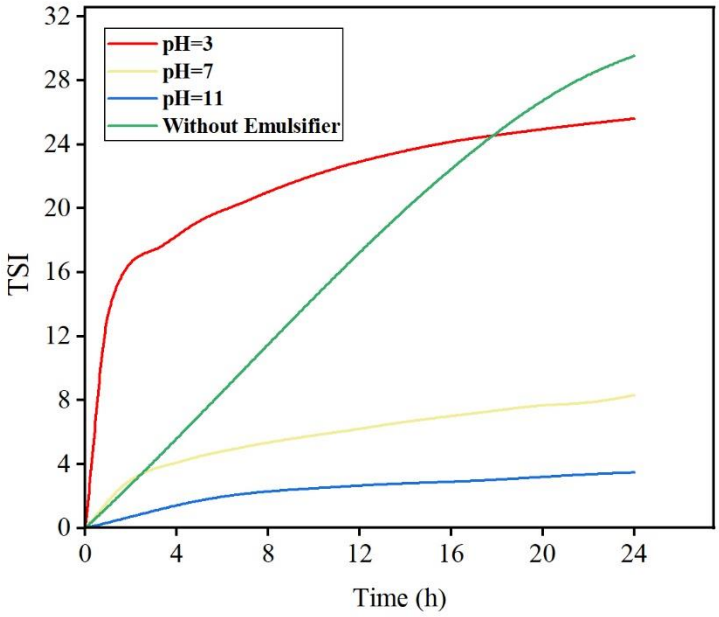

Fig. 4.6. TSI variations for emulsions at different pH levels after 24 h

4.1.1.4 Rheological Characteristics

The viscosity of oil-water emulsions with varying pH was assessed by measuring their response to shear rates, as shown in **Fig. 4.6.** It is evident that all emulsions exhibit non-Newtonian behavior, meaning their viscosity does not remain constant with changing shear rates. As depicted in the **Fig. 4.6**, we observed a more noticeable increase in viscosity at pH 7 and even more so at pH 3. Past research indicates that alterations in emulsion viscosity are primarily influenced by the interactions occurring among molecules or particles in the continuous phase and the surfaces of the oil droplets (Carrillo et al., 2012). For instance, Li et al. (2016) proposed that the ion-dipole attraction between carboxymethylated lignin (CML) molecules and kerosene oil droplets resulted in heightened fluid viscosity (Falco et al., 1974). The same principle likely applies to the increased viscosity of the water-olive oil emulsion in the presence of sulfonated lignin at pH 7. However, the significant

surge in emulsion viscosity at pH 3 indicates a much stronger interaction (such as favorable hydrophobic interaction and π-π stacking) between sulfonated lignin and olive oil (Li and Yang, 2015). Furthermore, a Pickering emulsion (formed from particles) generally exhibits high viscosity due to the adsorption of solid particles at the oil interface, which restricts the motion of oil droplets (Zhang et al., 2017).

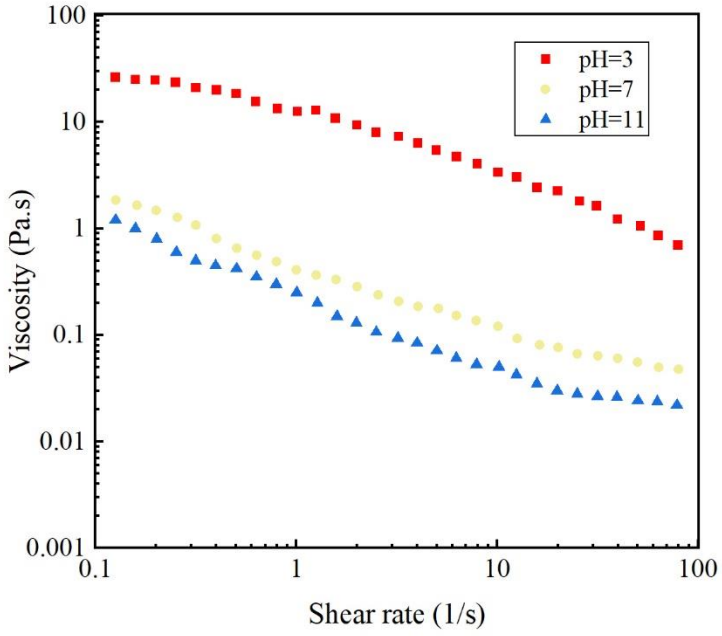

Fig. 4.7. Viscosity versus the shear rate of emulsions stabilized by sulfonated lignin at different pH of 3, 7, and 11

4.1.2 Sulfomethylated Kraft Lignin Properties and ^{1}H–NMR Spectroscopy

Fig. 4.7 (a) illustrates the synthetic process of sulfomethylated kraft lignin production. This reaction utilizes formaldehyde to introduce a methyl group, while sodium sulfite contributes a sulfonated group for sulfomethylation. The reaction mechanism involves electrophilic substitution, wherein, under alkaline conditions, the oxygen atoms' lone pair of electrons associated with the phenolic OH group is donated to the aromatic ring of lignin. Consequently, the ring gains a rich electron density, enabling the electrophilic substitution of the ring by the sodium methyl sulfonate group, resulting in the formation of sulfomethylated lignin (Konduri and Fatehi , 2015). It is essential to consider that there may be competing side reactions during the synthesis process, such as the generation of sodium thiosulfate, which can reduce the overall yield of sulfomethylated lignin. This is depicted in **Fig. 4.7 (b)**, highlighting the potential impact on the final product's yield (Madzhidova et al., 1998). One notable observation is that the charge density of modified lignin directly correlates with its sulfomethylated group content. Since the sulfomethylation reaction specifically affects the sulfomethylated groups attached to the lignin structure, any alterations in the sulfomethylated group content directly correspond to changes in the charge density of the modified lignin.

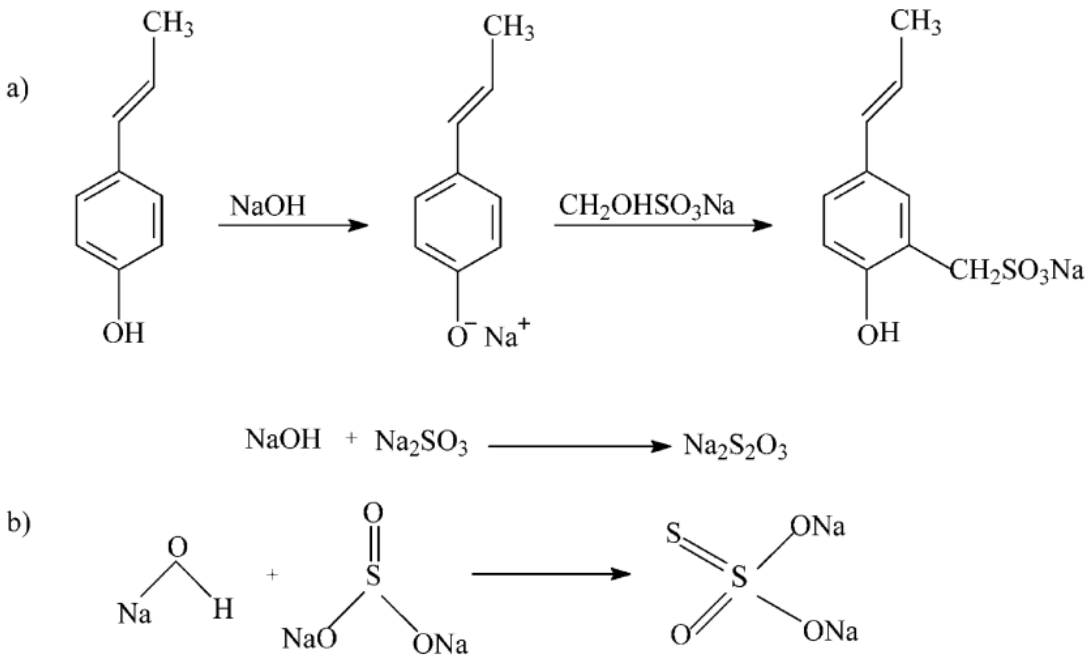

Fig. 4.8. (a) Sulfomethylation of lignin and (b) undesired sodium thiosulfate production.

The structures of kraft lignin and sulfomethylated lignin were examined using ^{1}H-NMR spectra in DMSO-d6, shown in **Fig. 4.9**. In all the spectra, the peak at 2.58 ppm is from DMSO-d6. For kraft lignin, there are two broad peaks: 6.8–7.5 ppm is from the aromatic ring protons, and 3.2–3.8 ppm is from the methoxy groups (Bahrpaima and Fatehi, 2018). In sulfomethylated lignin, these peaks are weaker due to sulfomethylation reactions breaking the aromatic ring and methoxy groups (He and Fatehi, 2015). The 8.2 ppm peak is from the phenolic hydroxy hydrogen present in both, suggesting that these hydroxyl groups remained unchanged during sulfomethylation. In sulfomethylated lignin, the 3.23 ppm peak indicates the presence of -CH2 groups resulting from sulfomethylation (Jiao et al., 2018).

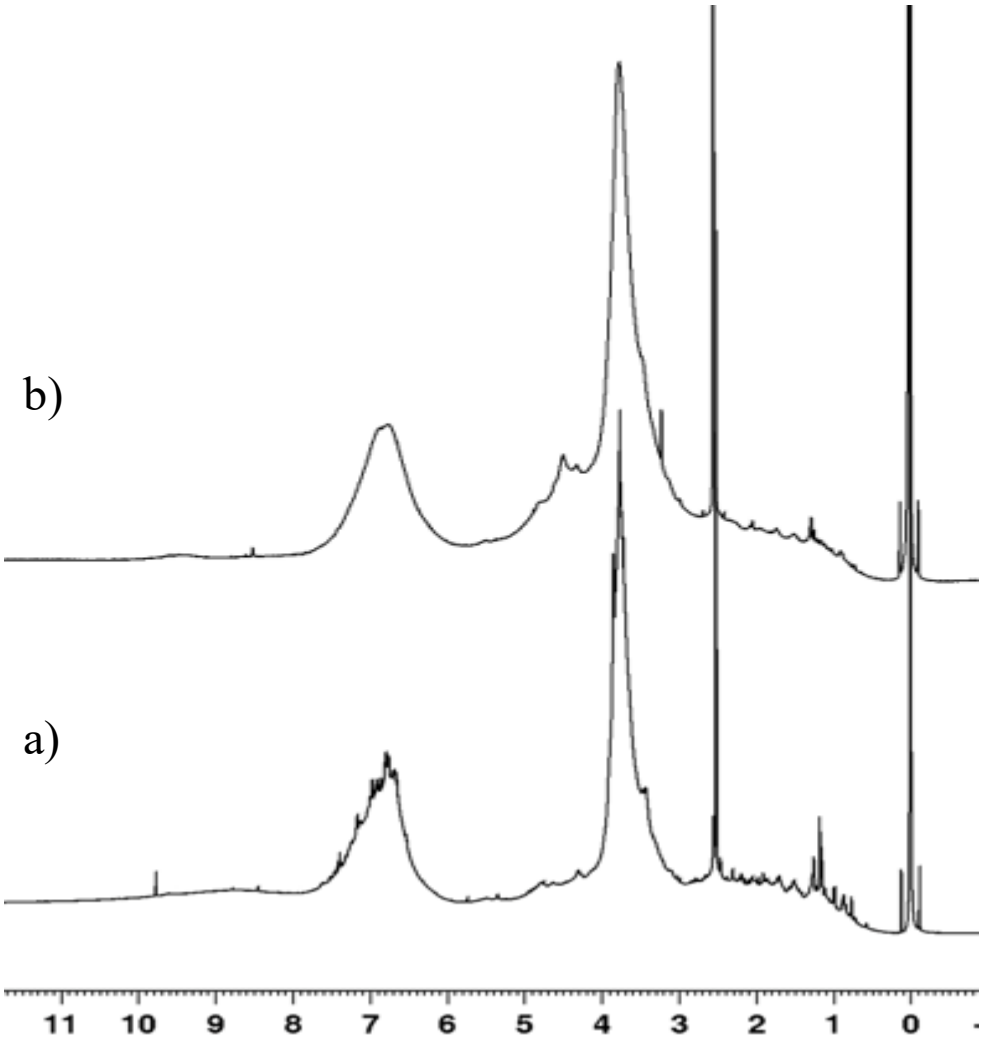

Fig. 4.9. ^{1}H–NMR Spectra of kraft lignin (a), sulfomethylated lignin (b) in DMSO-d6

This research aimed to investigate the impact of charge density on the emulsification performance of sulfomethylated kraft lignin. To achieve this, three variations of sulfomethylated kraft lignin were synthesized, each possessing a distinct charge density. To quantify this relationship, **Table 4.2** provides a comprehensive overview of the samples. The highest charge density among the samples was observed in HSML, with a value of 1.67 meq/g. LSML exhibited the lowest charge density of 1.18 meq/g on the other end of the spectrum. MSML represented the sample with a

medium charge density of 1.39 meq/g. The variance in charge density across these samples can be attributed to the varying reagent-to-lignin ratios employed during synthesis. In addition to the observations mentioned above, another noteworthy finding is that as the reagent ratio increases, the carbon composition decreases, indicating a reduction in the proportion of carbon atoms within the modified lignin structure. Conversely, both the sulfur content and molecular weight of the sulfomethylated lignin increase as the reagent ratio is elevated. This implies that a higher concentration of the reagents used in the sulfomethylation reaction leads to augmented incorporation of sulfur into the lignin structure **Table 4.2.** Properties of softwood kraft lignin and different Sulfomethylated kraft lignin and results in larger molecular weight chains within the modified lignin. Interestingly, despite these variations, the amount of phenolic OH groups remains constant regardless of the reagent ratio. This suggests that the sulfomethylation reaction primarily affects other functional groups within the lignin structure while maintaining the consistent presence of phenolic OH groups (Kazzaz et al., 2019).

Table 4.2. Properties of softwood kraft lignin and different Sulfomethylated kraft lignin

Sample	Reagent/lignin ratio (mole/mole)	Charge density (meq/g)	Solubility %	C%	H%	N%	S%	Molecular weight (g/mol)	Phenolic group (mmol/g)
Softwood Kraft lignin	-	-	37	64.84	7.09	0.09	1.23	-	0.5
HSML	3/1	1.67	100	52.24	6.59	0	3.97	4662	0.5
MSML	1/1	1.39	100	54.17	6.65	0	2.50	3866	0.5
LSML	0.5/1	1.18	100	57.7	6.37	0	1.70	3476	0.5

4.1.2.1 Contact angle measurements

The water contact angle (WCA) at the solid interface of various samples in an air-water environment was measured based on previous research (Hu and Russell, 2021). **Fig. 4.8 (a)** presents the recorded WCA values for three samples: HSML, MSML, and LSML. The findings reveal that the variation in charge density ranging from 1.18 to 1.67 had no discernible effect on the water contact angle. Interestingly, all three samples exhibited similar hydrophilic behavior, as indicated by WCAs of approximately 11°. **Fig. 4.8 (b)** illustrates how droplets from different solutions behave when they come into contact with a glass surface that is covered by oil. The sample with the highest charge density has a larger contact angle than the sample with a lower charge density. HSML is more hydrophilic, meaning it has a greater affinity for water. This increased hydrophilicity is due to a higher concentration of sulfonic groups in the HSML sample.

As a result, the droplet from the HSML solution spreads out less on the oil-covered glass, resulting in a larger contact angle.

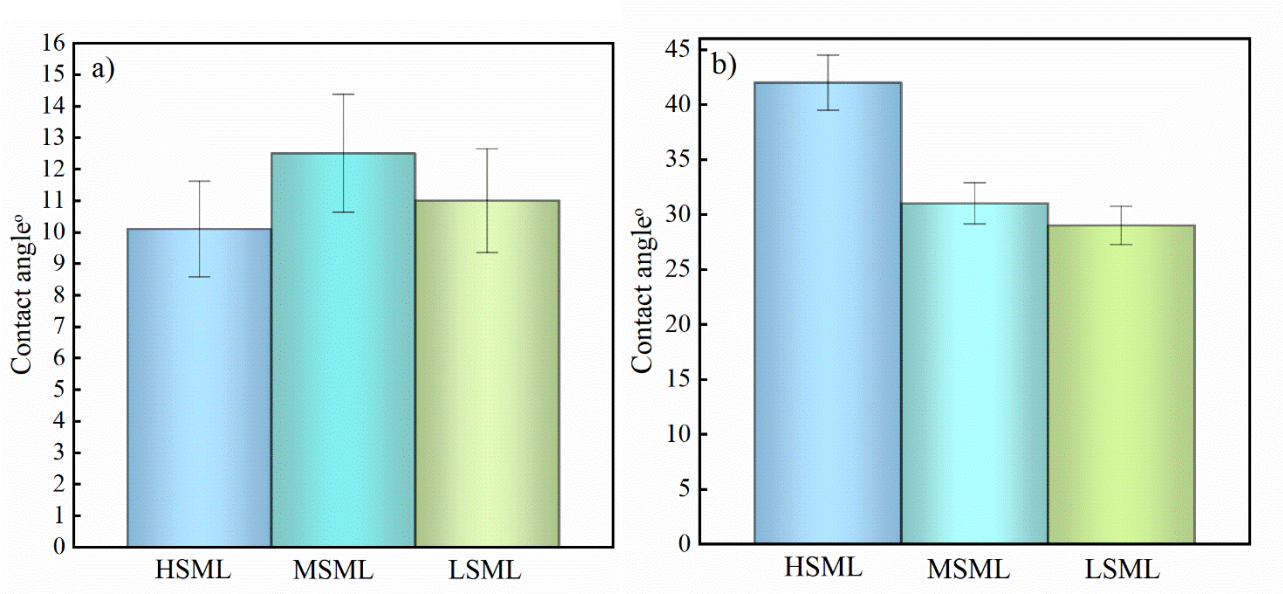

Fig. 4.10. (a) Water droplet contact angles of different sulfomethylated lignin-covered glass **(b)** Contact angle of different sulfomethylated lignin solutions droplets on the oil-covered glass

4.1.2.2 Emulsion Stability Assessment

In this research, emulsions were created using varying types of sulfomethylated lignin at a concentration of 0.25% and an equal ratio of oil to water. The stability of these emulsions, which were stabilized by different types of sulfomethylated lignin (HSML, MSML, and LSML), was tested over a 24 h period using a stability analyzer. The results of this test can be seen in **Fig. 4.10.** This figure demonstrates that altering the charge density of the emulsifier within the range of 1.18 to 1.67 does not noticeably impact the stability of emulsions. These findings are consistent with the results obtained from our rheology measurements (**Fig. 4.13, Fig. 4.14**).

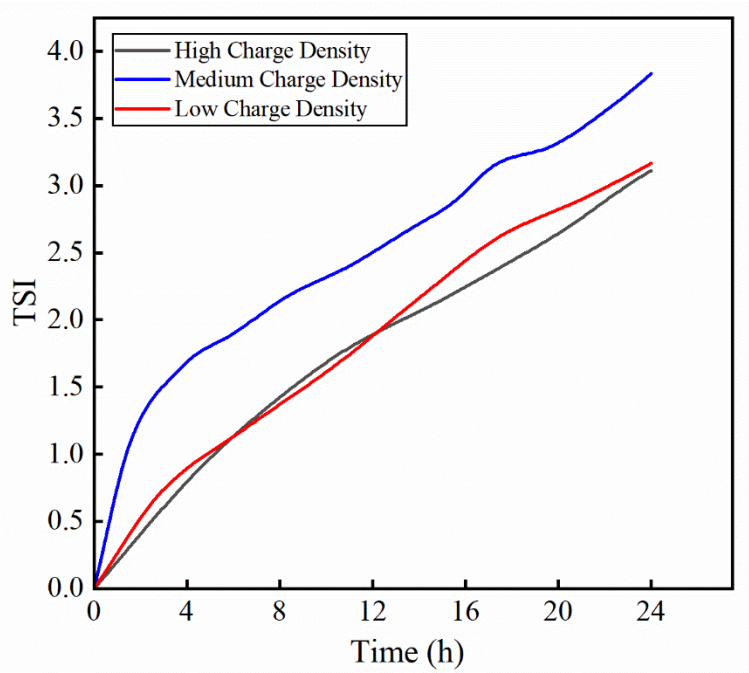

Fig. 4.11. TSI variations for emulsions stabilized by sulfomethylated lignin with different charge densities after 24 h

Apart from examining the impact of charge density on emulsion stability, the influence of emulsion temperature was also explored and depicted in **Fig. 4.11**. The results clearly indicate that as the temperature rises from 25°C to 40°C, the stability of the emulsion decreases, with the TSI reaching approximately 10.5 after 24 h. In contrast, at 25°C, the TSI reaches around 3.5. Increasing the temperature can reduce the stability of emulsions because it decreases the oil's viscosity, increases the collisions between droplets, and broadens the difference in density between different phases. This leads to weakening the interfacial film's mechanical strength surrounding the droplet and enhances the demulsification efficiency (Abdolmaleki et al., 2019; Jiao et al., 2022) . Temperature affects the physical properties of oil, water, interfacial films, and surfactant solubilities in the oil and water phases, affecting the emulsion's stability (Partal et al., 1997).

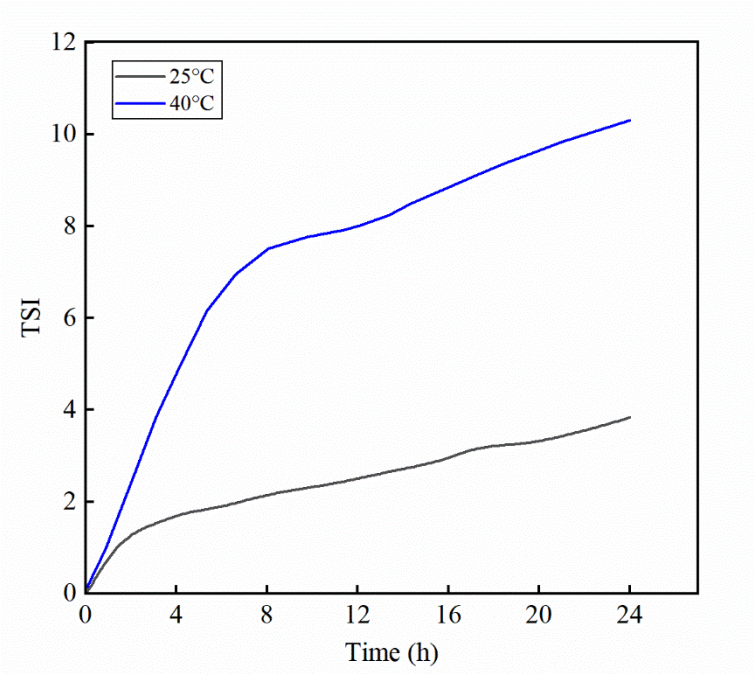

Fig. 4.12. TSI variation for emulsions stabilized by sulfomethylated lignin at different temperatures of 25°C, and 40°C after 24 h

Moreover, the stability of emulsions stabilized by sulfomethylated lignin was examined concerning emulsion pH, as presented in **Fig. 4.12**. The findings indicate that varying the pH from 3 to 11 does not significantly impact the stability of these emulsions. This can be attributed to the consistent solubility of sulfomethylated lignin across different pH levels. Furthermore, it was observed that the polymer solution remained stable even under acidic pH conditions.

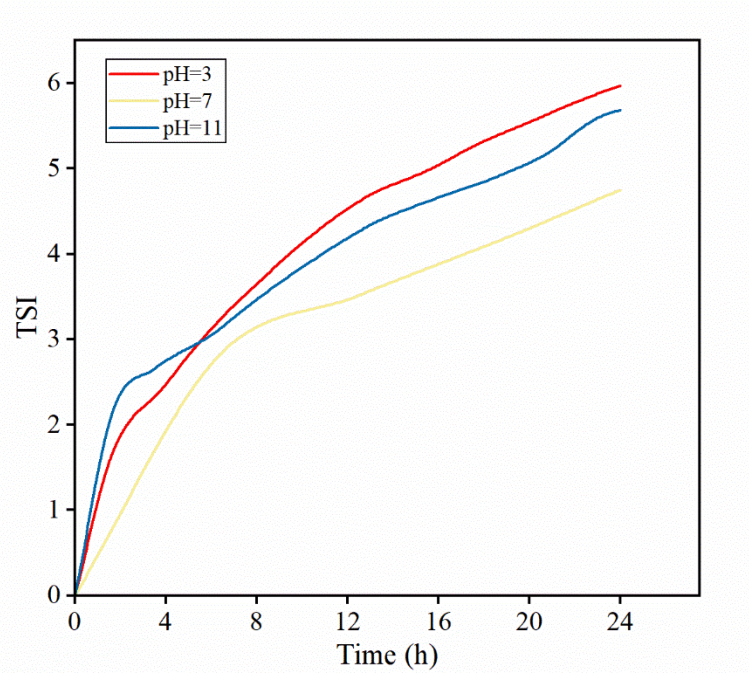

Fig. 4.13. TSI variation for emulsions stabilized by sulfomethylated lignin at different pH of 3, 7, and 11 after 24 h

4.1.2.3 Rheology Characteristics

Fig. 4.13 illustrates the influence of emulsifier charge density on the rheological properties, specifically the viscosity of the emulsions. The results indicate that altering the charge density within the range of 1.18 to 1.67 does not significantly affect the emulsions' viscosity. Furthermore, it is observed that all emulsions exhibit non-Newtonian behavior as their viscosity does not remain constant with changing shear rates (Rosti and Takagi, 2021).

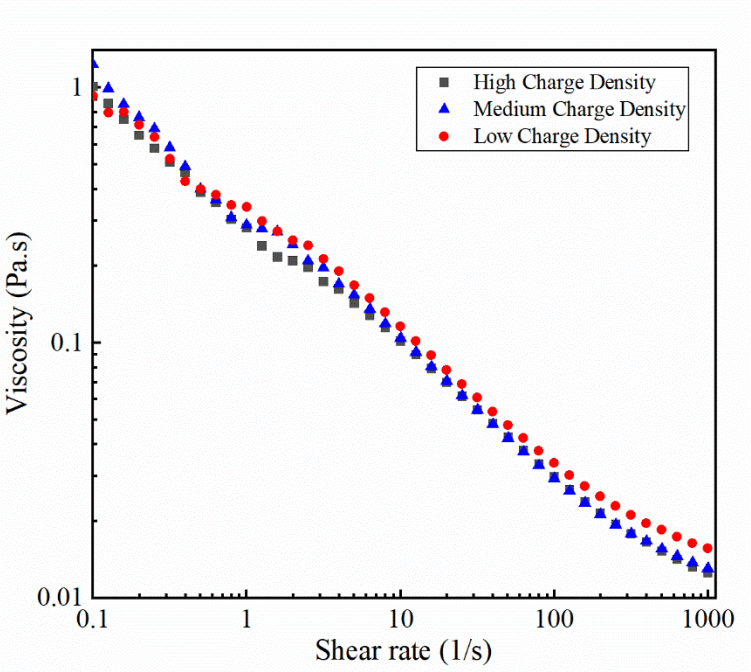

Fig. 4.14. Viscosity versus the shear rate of emulsions stabilized by sulfomethylated lignin with different charge densities

Oscillatory measurements are valuable for illustrating the viscoelastic characteristics of emulsions. The magnitudes of the storage and loss modulus depict two distinct behaviors: either a viscous, liquid-like behavior ($G' < G''$), or an elastic, gel-like behavior ($G' > G''$) (Xiao et al., 2019; Celia et al., 2009). **Fig. 4.14** illustrates the storage and loss moduli as a function of angular frequency for emulsions stabilized by sulfomethylated lignin with various charge densities while maintaining a fixed strain (1%). The findings demonstrate that, across all emulsions and for the entire range of angular frequencies, the loss modulus (G'') consistently surpasses the storage modulus (G'). No crossover point is observed, indicating a liquid-like behavior in the emulsions. These results suggest that the stabilized emulsions lack the strength to form a network when the angular frequency increases (Kim et al., 2013).

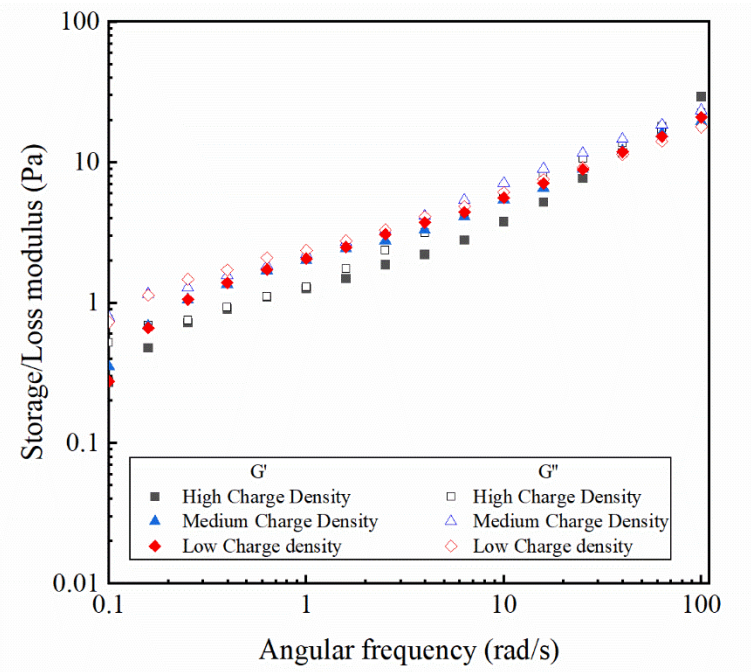

Fig. 4.15. Storage modulus G′ and loss modulus G″ versus angular frequency for emulsions stabilized by sulfomethylated lignin with different charge densities (G′ and G″ are represented as solid and open markers, respectively).

The rheological properties of oil-in-water emulsions are significantly affected by temperature. For instance, a study involving sunflower oil-in-water emulsions stabilized by gum tragacanth found that increasing the temperature from 5 to 50°C resulted in a fourfold decrease in the flow consistency index (Abdolmaleki et al., 2019). Similarly, another study observed a decrease in the viscosity of heavy crude oil over a temperature range of 25-65°C (Ghannam et al., 2012). To investigate the impact of temperature on the rheological properties, the viscosity of formulated emulsions was measured as a function of shear rates, and the results were presented in **Fig. 4.15**. There are noticeable viscosity differences among the emulsions at different temperatures. Consistent with previous studies, increasing the temperature led to a decrease in viscosity, further confirming the temperature-dependent nature of emulsion rheology.

.

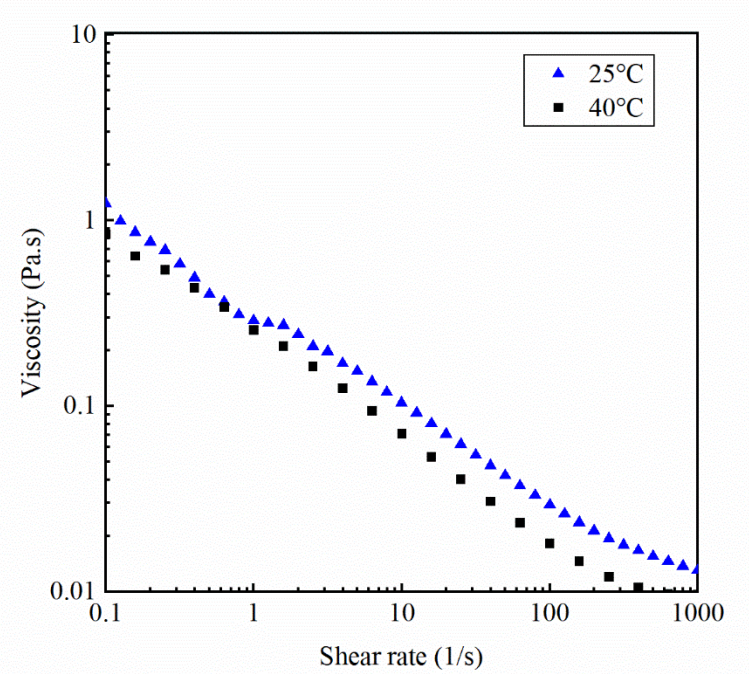

Fig. 4.16. Viscosity versus the shear rate of emulsions stabilized by sulfomethylated lignin at different temperatures of 25°C and 40°C

Fig. 4.16 presents the storage and loss modulus as a function of angular frequency for emulsions stabilized by sulfomethylated lignin at two different temperatures, 25°C and 40°C, while maintaining a fixed strain of 1%. The results indicate that, across both emulsions and the entire range of angular frequencies, the loss modulus (G″) consistently exceeds the storage modulus (G′). This absence of a crossover point suggests a liquid-like behavior in the emulsions. Additionally, an important finding is that increasing the temperature causes a decrease in both G′ and G″. The reduction in G′ with temperature can be attributed to the weakening of intermolecular interactions or the structural integrity of the emulsion. This leads to a diminished ability of the emulsion to form a stable network or gel-like structure.

Consequently, the emulsion becomes less elastic and more fluid-like. Similarly, the decrease in G″ with temperature suggests a reduction in internal friction within the emulsion. This implies that the emulsion experiences reduced resistance to flow or deformation as the temperature rises.

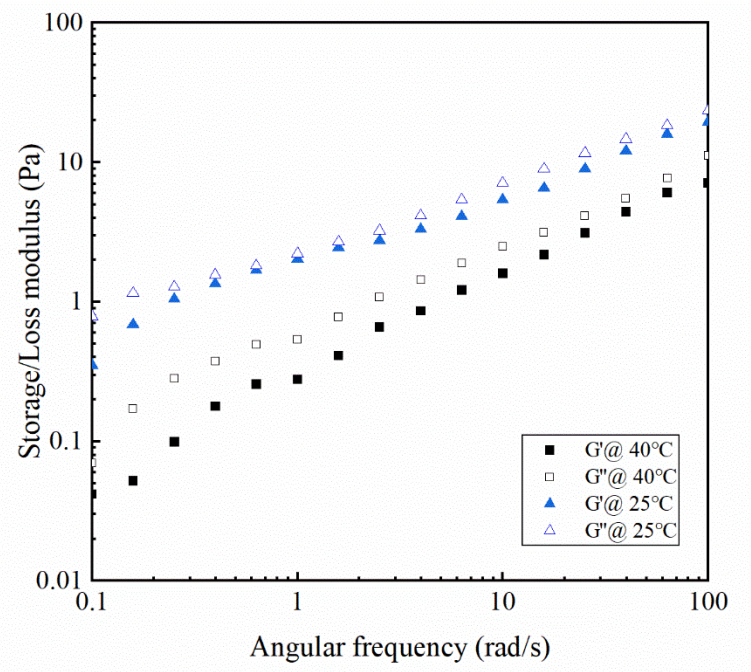

Fig. 4.17. Storage modulus G′ and loss modulus G″ versus angular frequency for emulsions stabilized by sulfomethylated lignin at different temperatures of 25°C and 40°C (G′ and G″ are represented as solid and open markers, respectively).

Fig. 4.17 presents the impact of emulsion pH on viscosity concerning shear rate, and **Fig. 4.18** depicts the storage and loss modulus as functions of angular frequency, respectively. The results suggest that varying the pH within the range of 3 to 7 and 11 does not significantly affect the rheological properties of the emulsions. This observation can be attributed to the stability and solubility of sulfomethylated lignin across this entire pH range of 3 to 11.

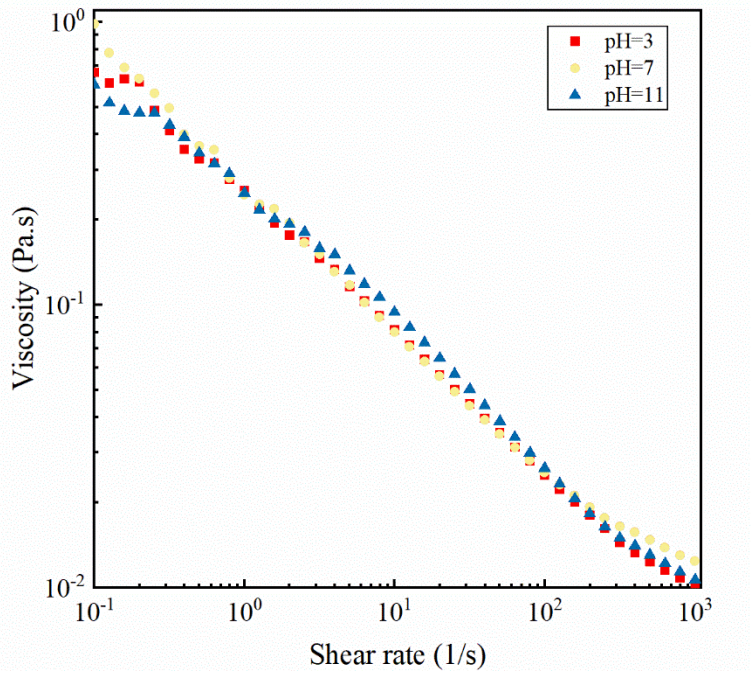

Fig. 4.18. Viscosity versus the shear rate of emulsions stabilized by sulfomethylated lignin at different pH of 3, 7, and 11

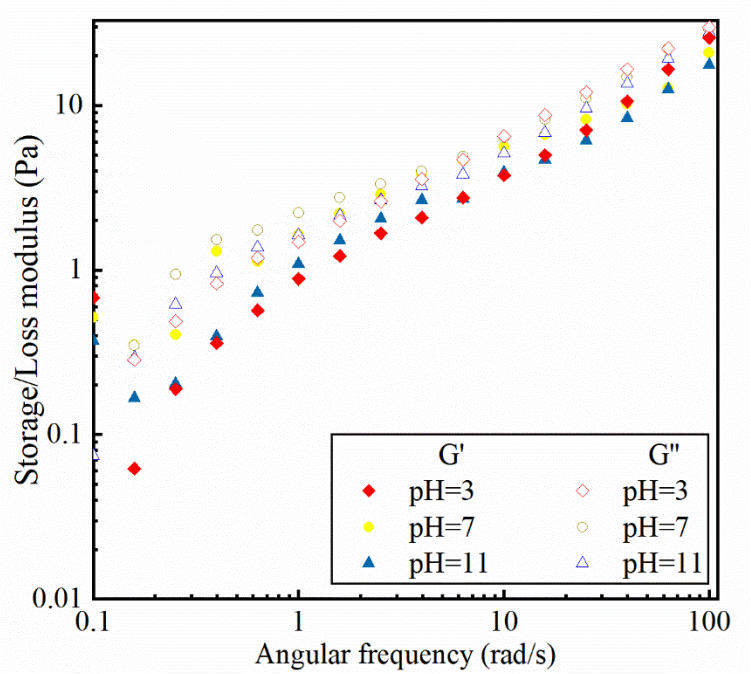

Fig. 4.19. Storage modulus G′ and loss modulus G″ versus angular frequency for emulsions stabilized by sulfomethylated lignin at different pH of 3, 7, and 11 (G′ and G″ are represented as solid and open markers, respectively).

4.2 Mixing

In various industrial processes, selecting suitable mixing equipment is crucial for efficiency and the quality of the final product, where the mean diameter and the droplet size distribution play a critical role. Therefore, the results of the study are presented in two parts. The first part focuses on the impact of impeller speed, impeller type, oil-water ratio, and oil type in a stirred tank on the mean diameter and droplet size distribution. The second part addresses the effects of amplitude and frequency in a batch oscillatory baffled reactor on the mean diameter and droplet size distribution.

4.2.1 Stirred Tank

- Effect of Impeller Speed

The final drop size distribution is indicated when there is no further change in mean diameter during a breakage and coalescence in a mixing tank. This means a dynamic equilibrium between drops has been reached (Zainal Abidin, M. I. I.et al., 2014; Hiraoka, S. et al., 2001). The Sauter mean diameter, also referred to as d_{32}, serves as a defining factor utilized to depict the average size of particles in a dispersion of varying particle sizes. In other words, it represents the size at which the total volume of particles in the distribution is evenly distributed. Essentially, it signifies the dimension at which the total volume of particles within the distribution achieves uniformity. This parameter is really important, especially in studies about making emulsions. It helps us know how everything is spread out, how important it is for keeping things stable, and it's also easy to use for comparing results and talking about them clearly (Zeng et al., 2015).

Fig. 4.19 displays the influence of three different impeller speeds of 150, 200, and 250 rpm on the Sauter mean diameter over time until a dynamic equilibrium is achieved at $\varphi = 2.5\%$ canola oil

with a radial impeller used in all trials. Increasing the impeller speed can raise the flow velocity gradient, which, in turn, enhances the likelihood of oil droplet breakage. Increased agitation speed can also cause turbulent pressure fluctuations to rise, creating turbulent eddies that can supply enough energy for breaking up droplets (Stamatoudis M. and Tavlarides L.,1987). Additionally, smaller droplets are generated as the stirring time increases until the droplet breaking and coalescence process reaches a steady state.

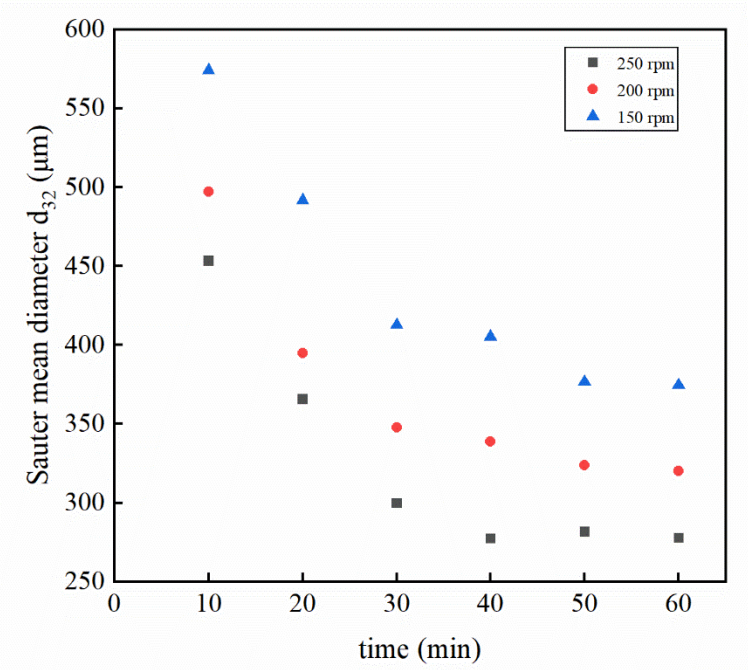

Fig. 4. 20. Transient Sauter mean diameter at three different impeller speeds ($\varphi = 2.5\%$ canola oil, radial impeller)

Fig. 4.20 presents the droplet size distribution curves achieved by a radial impeller when 2.5% canola oil was used, varying the impeller speeds to 150, 200, and 250 rpm. As demonstrated in **Fig. 4.19**, increasing the impeller speed increased the fraction of oil droplets with a small diameter, causing the distributions to shift to smaller sizes. The mean droplet size after 60 minutes of mixing changed from 374.5 μm at 150 rpm to 320 μm at 200 rpm, then to 277.7 μm at 250 rpm, and finally

to 60.84 μm at 250 rpm. Alopaeus et al. (2002) and Boxall et al. (2010) also observed a shift in droplet size distributions due to an increased agitation speed.

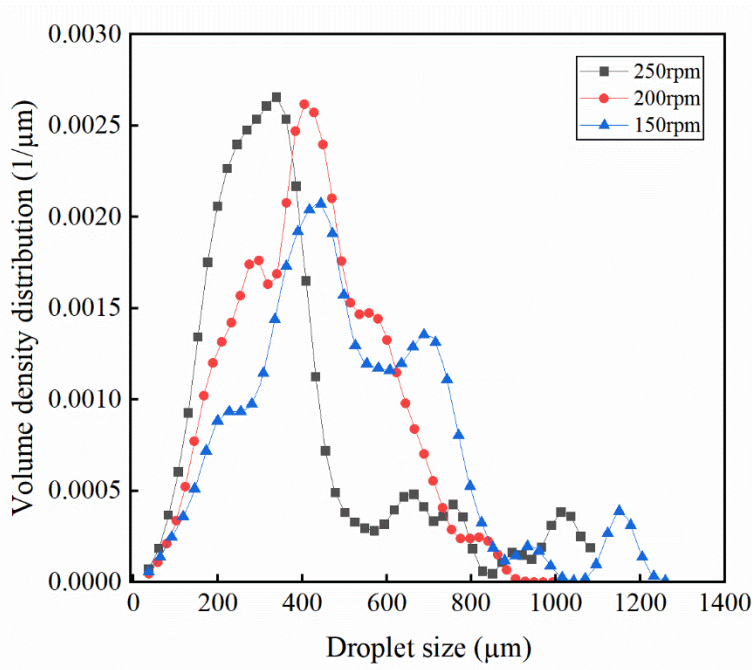

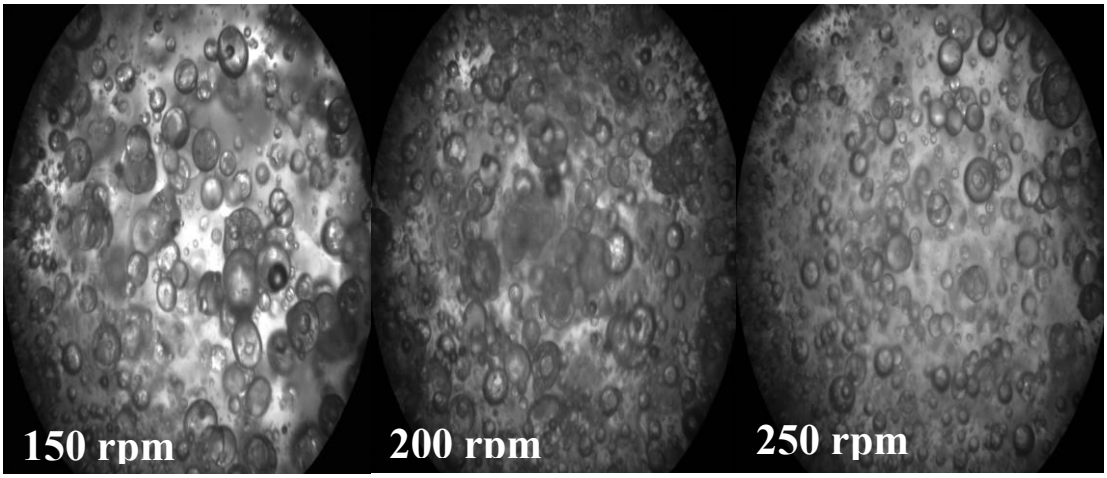

Fig. 4. 21. Effect of impeller speed on droplet size distribution ($\varphi = 2.5\%$ canola oil, radial impeller) and their corresponding sample images

- Effect of Impeller Type

Most of the published research on liquid-liquid mixing has been conducted using the Rushton turbine. By comparing various impeller designs, researchers can make an informed decision regarding the most suitable choice for a liquid-liquid mixing process. **Fig. 4.21** illustrates a comparison of the achieved Sauter mean diameter using different types of impellers after 60 minutes of mixing with different impeller speeds. The findings demonstrate that the axial impeller consistently yields larger d_{32} values at identical energy dissipation rates or impeller speeds, whereas the radial impeller yields the smallest d_{32}. This discrepancy can be attributed to the influence of shear stress on droplet size within a mixture, which is determined by the type of impeller utilized. Due to their specific design and operational characteristics, radial impellers generate higher shear rates than axial or radial-axial impellers (Spicer et al., 1996). This heightened shear results in smaller droplet sizes within the mixture. This phenomenon arises from the flow patterns generated by different impeller types. Radial impellers generate an outward (in radial direction), high-velocity flow that induces significant turbulence, generating high shear forces. These forces effectively break down larger droplets into smaller ones, reducing the average droplet size. A radial impeller disperses one liquid into another.

In contrast, axial and radial-axial impellers generate a flow pattern along the impeller's axis. This flow pattern produces less turbulence and lower shear forces than radial impellers. Consequently, larger average droplet sizes are observed in mixtures stirred by axial and radial-axial impellers (Giapos et al., 2005; Ghotli et al., 2019; Zhou and Kresta, 1996).

Fig. 4.22 illustrates the impact of impeller type on droplet size distribution at a constant impeller speed of 250 rpm. As anticipated, the droplet size distribution is narrower and shifted towards smaller droplet sizes when using a radial impeller compared to the axial and axial-radial impellers.

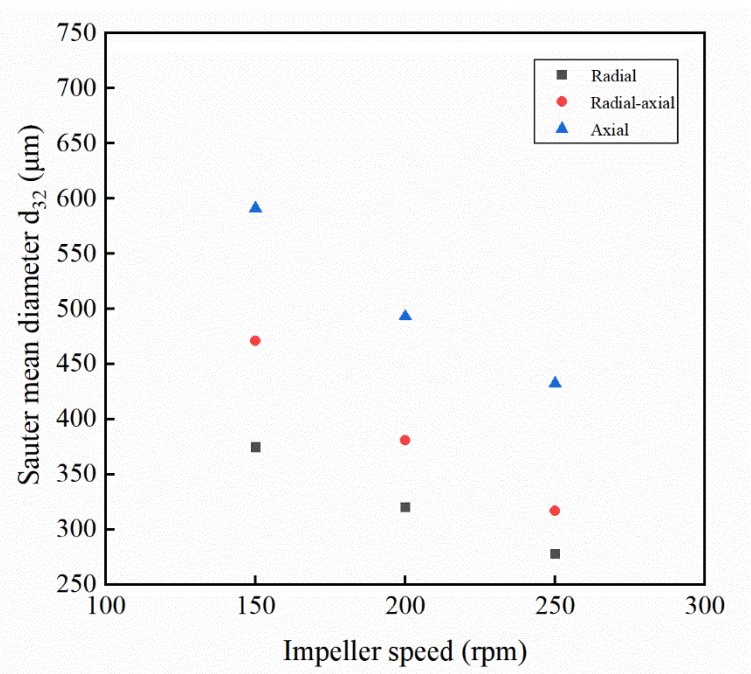

Fig. 4.22. Effect of impeller type on Sauter mean diameter at different impeller speeds ($\varphi =$ 2.5% canola oil)

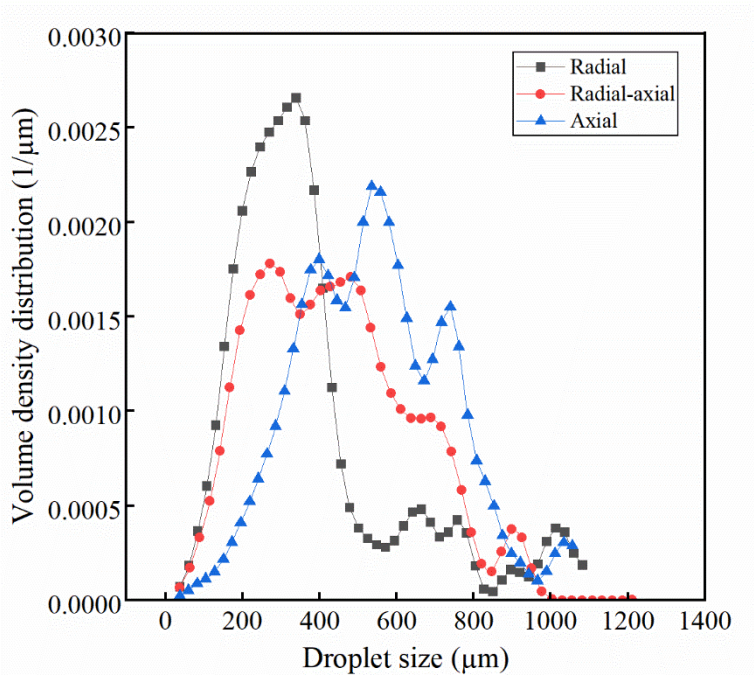

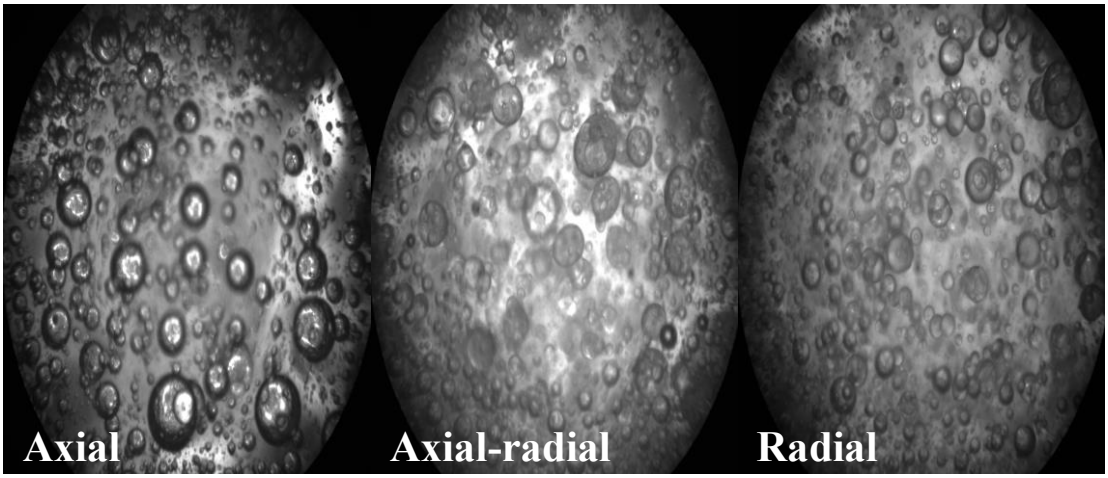

Fig. 4.23. Effect of impeller type on droplet size distribution ($\varphi = 2.5\%$ canola oil, 250 rpm) and their corresponding sample images

- Effect of Oil Volume Fraction

Fig. 4.23 depicts the relationship between the Sauter mean diameter and impeller speed for different volume fractions of canola oil. It is evident from the figure that the Sauter mean diameter decreased as the impeller speed increased, regardless of the volume fraction of the oil. However,

lower Sauter mean diameters were achieved with lower volume fractions at a constant impeller speed. The oil's viscosity, which serves as the dispersed phase, is higher than water, which acts as the continuous phase. Consequently, as the oil volume fraction decreases, the overall mixture viscosity decreases (Nagata ,1975). A higher volume fraction of the dispersed phase leads to increased drag force between the phases, reducing turbulence within the tank (Zhao et al., 2011)

Fig. 4.24 demonstrates the impact of volume fractions on the droplet size distribution of canola oil at a constant agitation speed of 250 rpm using a radial impeller. Interestingly, although 2.5% and 5% oil volume fractions exhibited a similar trend, with minimal changes in droplet size distribution, slightly narrower distributions were observed at lower volume fractions.

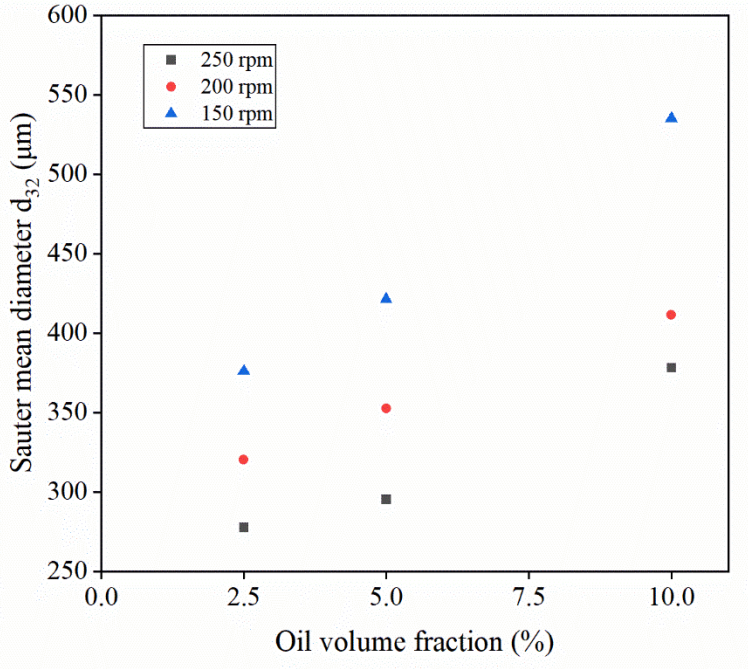

Fig. 4.24. Effect of oil volume fraction on Sauter mean diameter at different impeller speeds (canola oil, radial impeller)

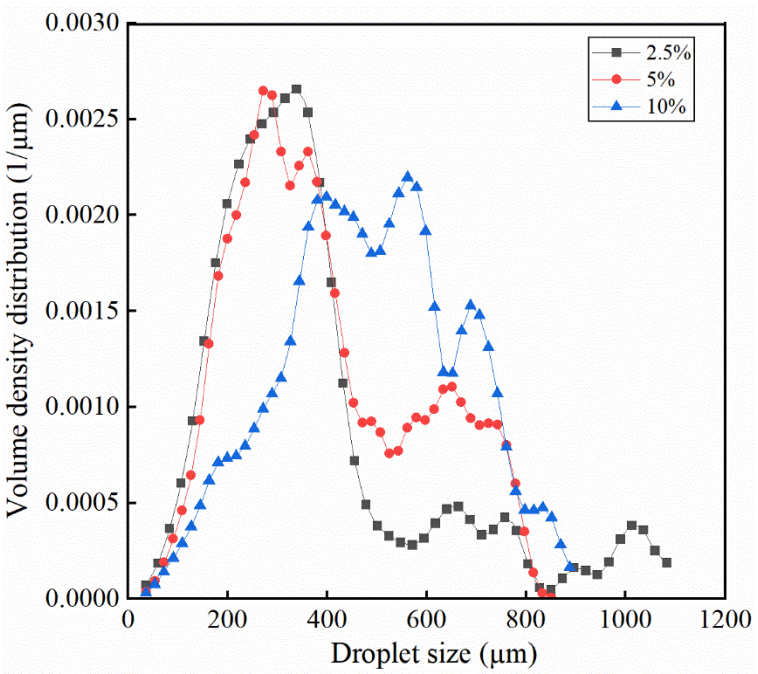

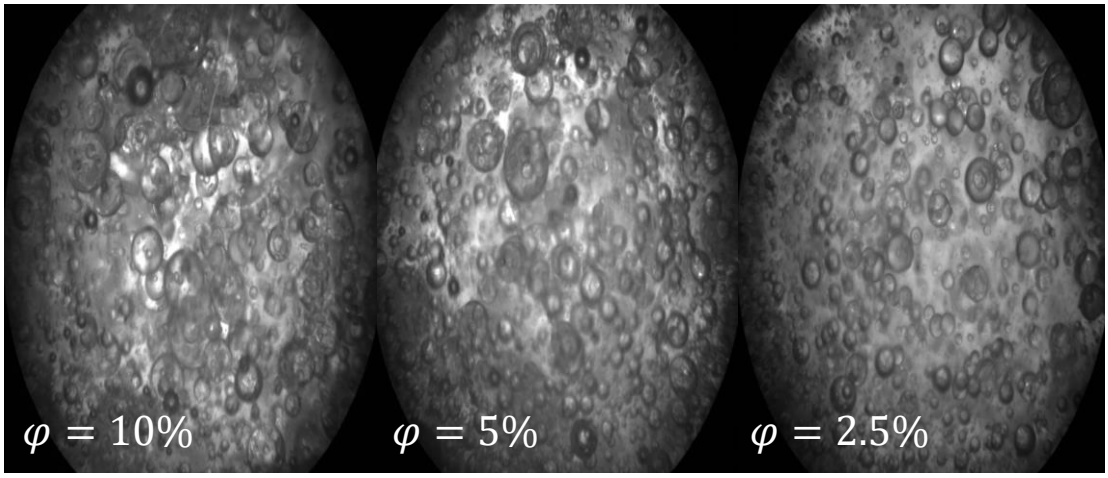

Fig. 4.25. Effect of oil volume fraction on droplet size distribution (canola oil, 250 rpm, radial impeller) and their corresponding sample images

- Effect of Oil Type

In commercial applications, various oils create emulsion-based beverages and foods. When formulating stable emulsion-based delivery systems, an essential consideration is choosing the right type of oil phase (McClements et al., 2007). Therefore, the influence of different oil types on droplet size distribution was investigated. **Fig. 4.25** displays the Sauter mean diameter of droplets for canola and olive oils at various impeller speeds. The results indicate a consistent trend where increasing the impeller speed reduces the Sauter mean diameter, irrespective of the oil type. Additionally, it is evident that olive oil generates larger droplet sizes at a constant impeller speed, resulting in a larger Sauter mean diameter than canola oil.

In **Fig. 4.26**, the droplet size distribution of canola and olive oil was compared at a 2.5% volume fraction and radial impeller speed of 250 rpm. Olive oil shifted towards larger oil droplet sizes and a narrower droplet size distribution. As indicated in **Table 3.1**, the interfacial tension of canola oil was similar to olive oil. Generally, increasing interfacial tension hindered the drainage of the liquid film between approaching droplets by increasing the interfacial rigidity (Dowding et al., 2001). Consequently, there is less coalescence observed among the liquid droplets.

Furthermore, droplet breakage requires the surrounding pressure to surpass the Laplace pressure $\Delta P = 2\sigma/r$, which is the pressure difference between the inside and outside of a droplet, determined by the interfacial tension (γ) and droplet radius (r) (Fragkopoulos et al., 2017). Therefore, higher interfacial tension results in higher Laplace pressure. In this study, the higher viscosity of olive oil contributes to a lower breakage rate, increasing droplet size. Increasing the viscosity of a liquid reduces the turbulent kinetic energy generated by impeller rotation (Gréa et al., 2014). Therefore, achieving smaller droplet sizes with olive oil requires more agitation, which can be accomplished by increasing the impeller speed. Consequently, the droplet size distribution

is influenced by the interaction between the viscosity of the dispersed phase and the interfacial tension, with the viscosity having the most significant impact. Naeeni and Pakzad ,(2019) also observed a change in droplet size distributions resulting from the interaction between interfacial tension and viscosity.

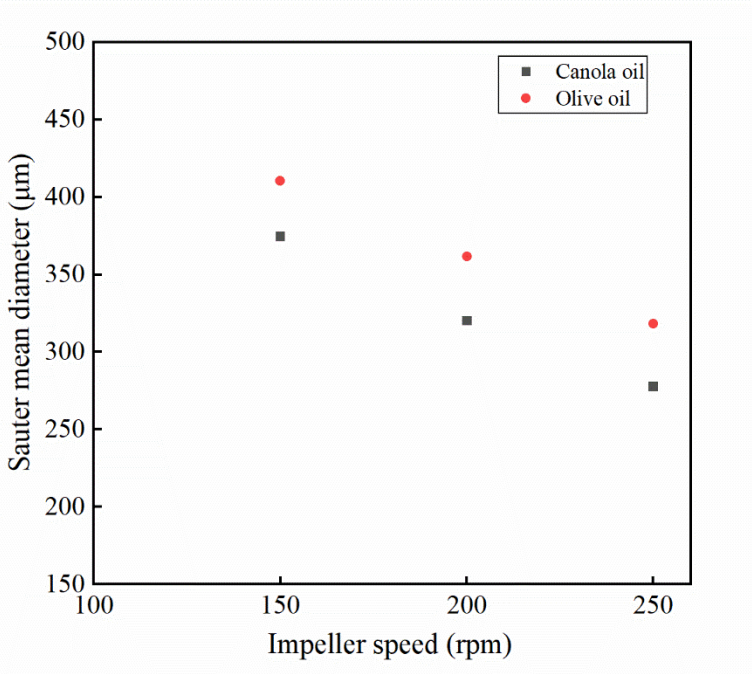

Fig. 4.26. Effect of oil type on Sauter mean diameter at different impeller speeds ($\varphi =$ 2.5% canola oil, radial impeller)

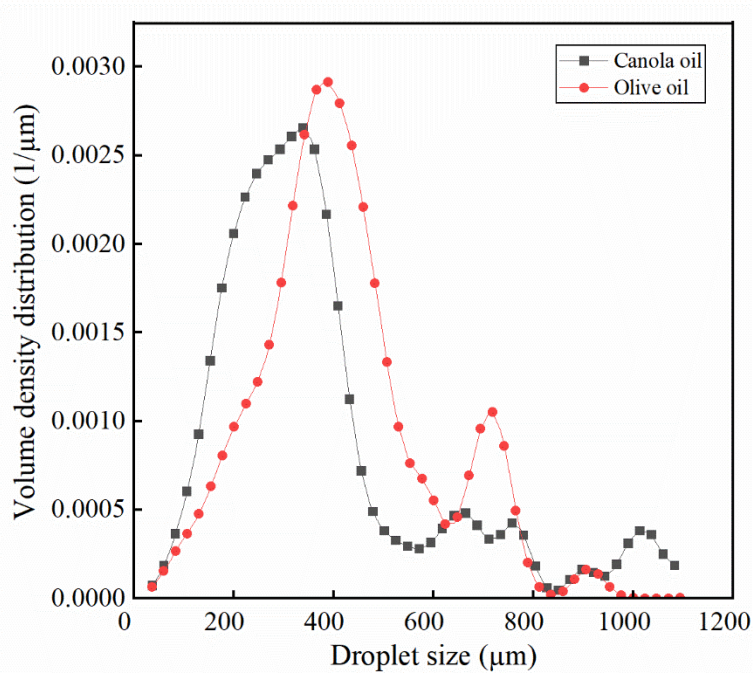

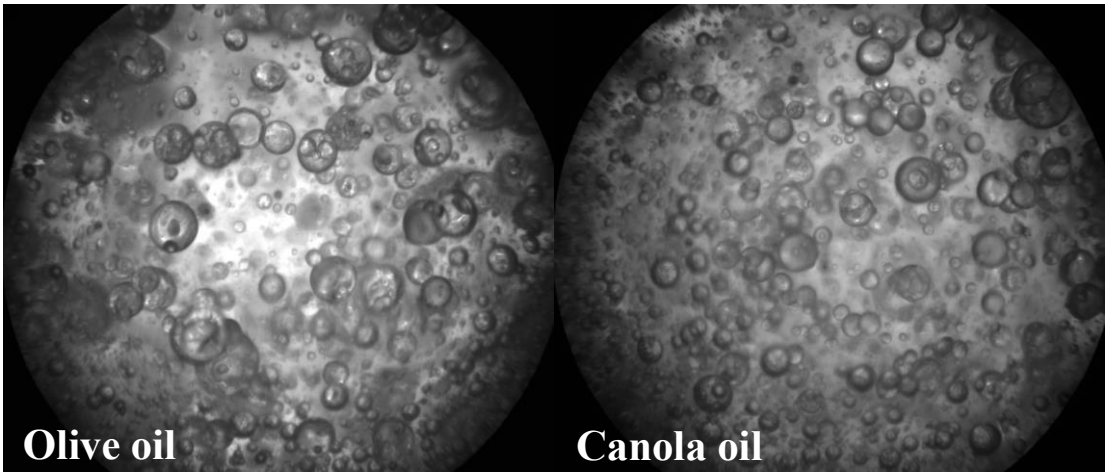

Fig. 4.27. Effect of oil type on droplet size distribution ($\varphi = 2.5\%$ canola oil, 250 rpm, radial impeller) and their corresponding sample images

4.2.2 Oscillatory Baffled Reactor

- Effect of Oscillation Amplitude

This study aimed to investigate the influence of amplitude on the Sauter mean diameter and droplet size distribution while maintaining a frequency constant (f=3 Hz, f=2 Hz). The results revealed that as the oscillation amplitude increased from 9 mm to 18 mm and 27 mm, there was a corresponding reduction in the Sauter mean diameter, as depicted in **Fig. 4.27**. Additionally, **Fig. 4.28** illustrates the droplet size distribution for each amplitude after one hour, indicating a shift towards smaller droplet sizes and a resulting narrower distribution. These findings demonstrate that increasing the oscillation amplitude while keeping the frequency constant effectively enhances droplet uniformity, decreasing the mean size. These outcomes align with prior studies by Lobry et al. (2015) and Ni et al. (1998). This observed trend can be attributed to the relationship between amplitude and the average energy dissipation rate, which, in turn, influences the turbulent intensity involved in the process of droplet breakage.

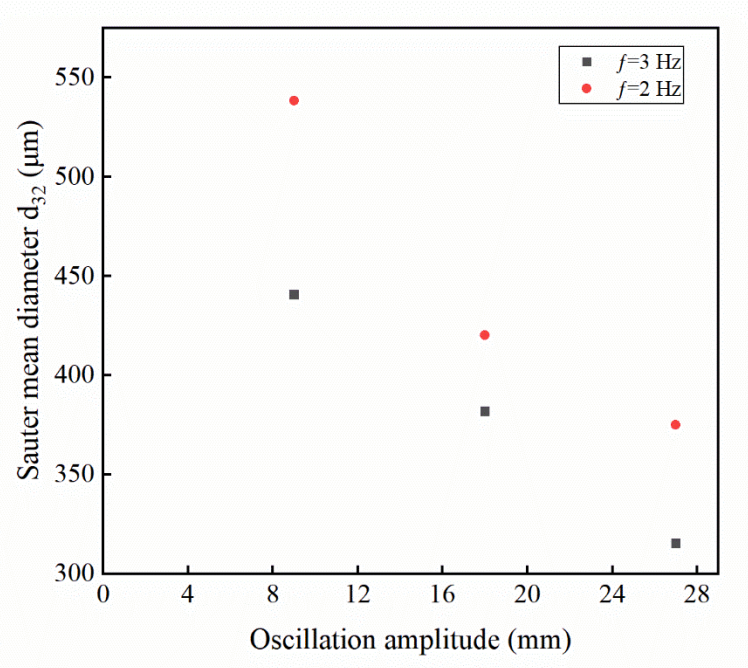

Fig. 4. 28. Effect of oscillation amplitude on Sauter mean diameter ($\varphi = 2.5\%$ canola oil, oscillation frequency = 3 and 2Hz)

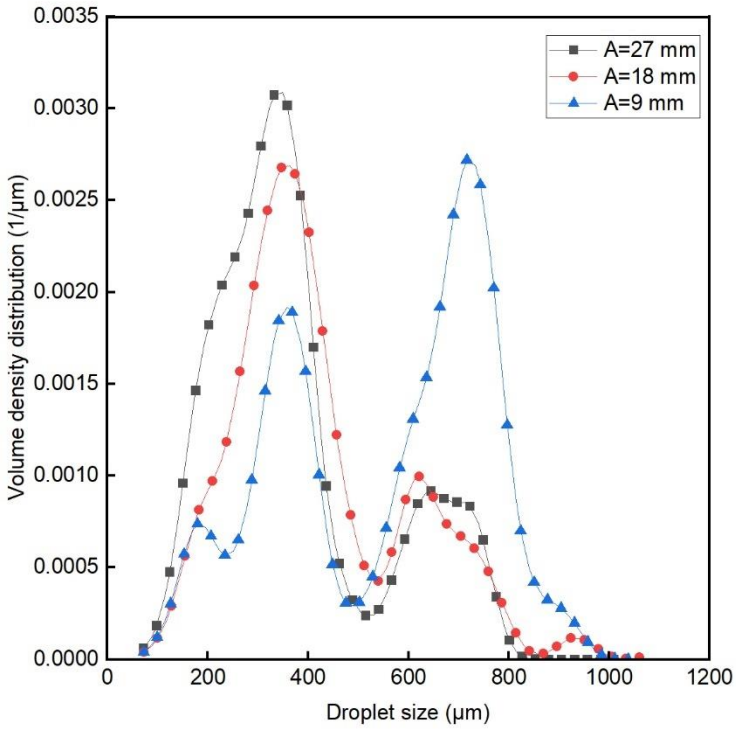

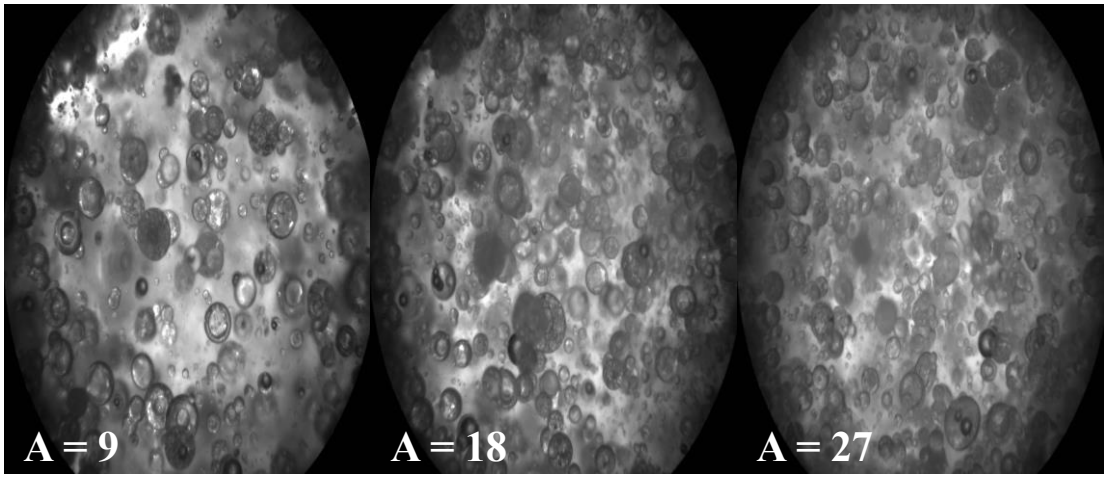

Fig. 4.29. Effect of oscillation amplitude on droplet size distribution ($\varphi = 2.5\%$ canola oil, oscillation frequency = 3 Hz) and their corresponding sample images

- Effect of Oscillation Frequency

The frequency (f) is another crucial aspect of the oscillation conditions. Similar to the amplitude, increasing the frequency from 1 Hz to 2 Hz and 3 Hz while keeping amplitude constant (A=27 mm, A=18 mm) leads to a decrease in the Sauter mean diameter d_{32}, as illustrated in **Fig. 4.29**. Also, **Fig. 4.30** demonstrates the impact of oscillation frequency on the size distribution of droplets. It can be observed that as the frequency of oscillation increases, the droplet distributions become narrower. This trend is similar to the findings in **Fig. 4.28**, which depicted the effect of the oscillation amplitude. Overall, increasing either the oscillation amplitude or frequency results in the production of more uniformly sized droplets in the OBR and these results were also reported by Pereira (2002) and Lobry et al. (2015) in a horizontally oriented continuous oscillatory baffled reactor.

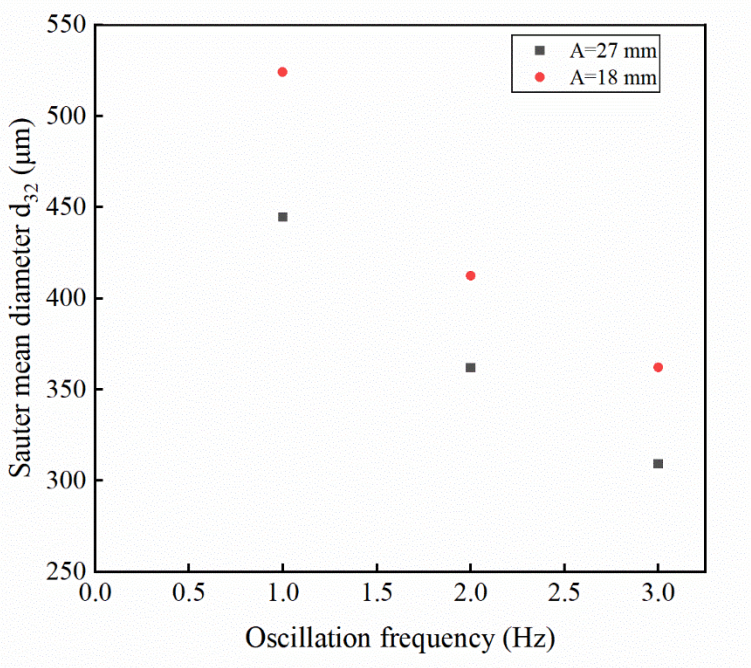

Fig. 4.30. Effect of oscillation frequency on Sauter mean diameter ($\varphi = 2.5\%$ canola oil, oscillation amplitude = 27 Hz, 18Hz)

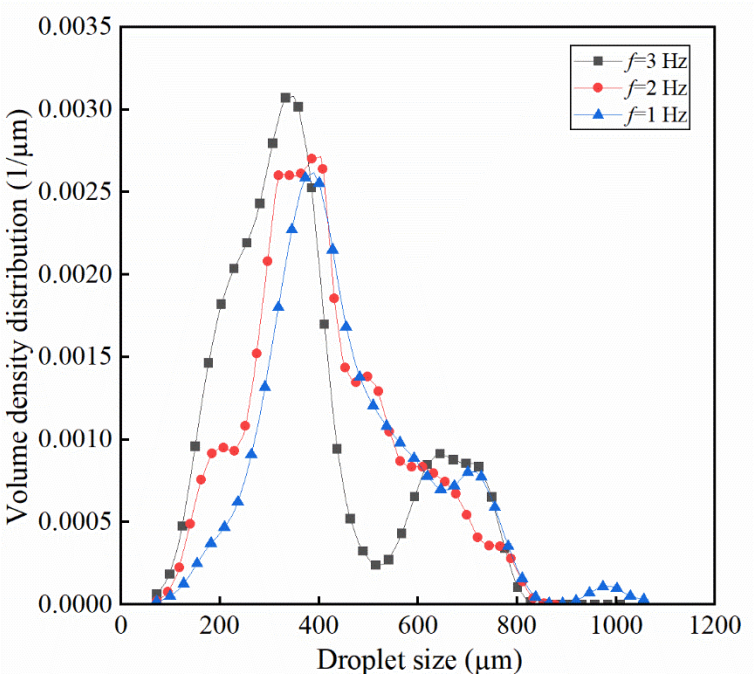

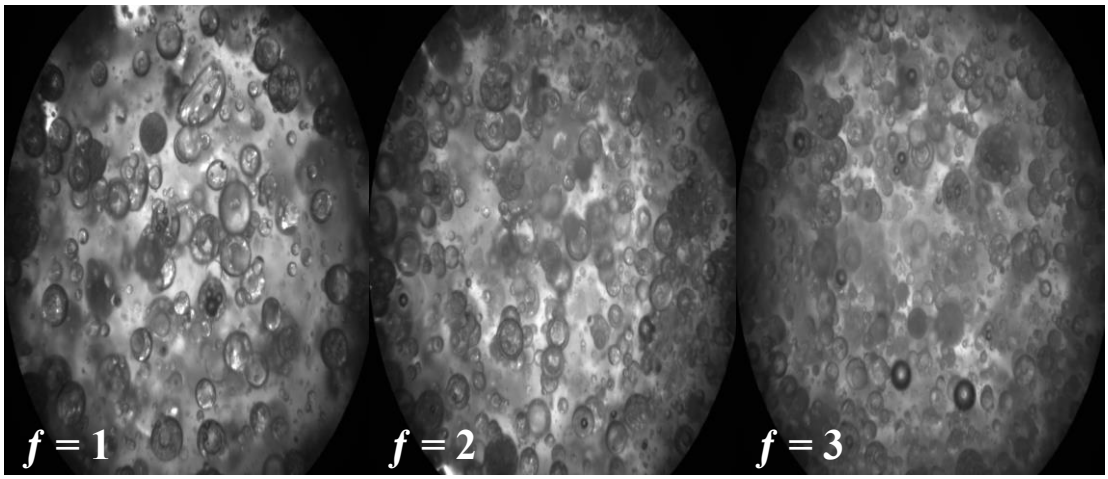

Fig. 4.31. Effect of oscillation frequency on droplet size distribution (φ = 2.5% canola oil, the oscillation amplitude = 27 Hz) and their corresponding sample images

Overall Conclusions and Recommendations

This work focused on controlling and customizing emulsion properties using environmentally friendly lignin-based emulsifiers. The process emphasizes sustainability by avoiding using solvents or hazardous chemicals in synthesizing sulfoalkylated lignin polymers. The synthesized sulfonated kraft lignin exhibited unique properties suitable for diverse applications. The polymer's charge density suggests the presence of charged groups, which is enabling interactions based on charge. Zeta potential measurements underscore the pH's role in stability determination, with higher pH values promoting stability through electrostatic repulsion. The study of emulsion stability revealed pH-dependent behavior of emulsifier, wherein higher pH levels correlated with enhanced stability, a finding substantiated by time-dependent variations in Turbiscan Stability Index (TSI). Rheological assessments revealed non-Newtonian behavior, influenced by interactions between polymer molecules and oil droplets. Overall, the research demonstrates the potential of lignin-derived emulsifiers to tailor emulsion properties sustainably and underscores the importance of pH in influencing stability and behavior.

Moreover, the study involved the synthesis of sulfomethylated kraft lignin with different charge densities. Water contact angle measurements consistently showed hydrophilic characteristics across all tested samples. Emulsion stability evaluation indicated that variations in charge density from 1.18 to 1.67 had minimal effects on stability. The rheological analysis revealed non-Newtonian behavior, emphasizing that the viscosity reduction was temperature-dependent. Higher temperatures led to reduced stability and a shift towards more fluid-like behavior in the emulsions. This comprehensive examination offers insights into the behavior of sulfomethylated kraft lignin-

based emulsions, shedding light on their stability, rheology, and response to different environmental conditions.

The second part of the study investigated the droplet size and droplet size distribution (DSD) in an un-baffled stirred tank and an oscillatory baffled reactor (OBR) using a dilute liquid-liquid dispersion. The SOPAT probe was effectively utilized for real-time monitoring and droplet size measurements. The experimental results provided insights into the effects of impeller speed, impeller type, oil-water ratio, oil type, oscillation amplitude, and frequency on droplet size and size distribution. In the stirred tank experiments, it was observed that increasing the impeller speed led to a decrease in the Sauter mean diameter and a shift toward smaller droplet sizes. Using a radial impeller promoted the formation of more uniform droplets and smaller droplet sizes. The dispersed phase volume fraction had a negligible effect on the droplet size distribution in diluted liquid-liquid dispersions.

Furthermore, the impact of oil type on droplet size distribution was investigated, revealing that different oils exhibited variations in droplet size and size distribution. In the oscillatory baffled reactor experiments, it was found that increasing the oscillation amplitude while keeping the frequency constant decreased the mean droplet size and narrower distribution. Similarly, increasing the oscillation frequency while maintaining the amplitude constant reduced the mean droplet size and a narrower distribution. These findings emphasize the importance of selecting appropriate mixing equipment and operating conditions for achieving desired droplet size and size distribution in various industrial processes. The results contribute to understanding the factors influencing droplet behavior in liquid-liquid dispersions, facilitating the design and optimization of mixing systems for improved efficiency and product quality.

Recommendations for Future Works

- Lignin's modification potential: Lignin can undergo modifications involving diverse cationic charge groups, such as aminaion of lignin.
- Emulsification assessment: Evaluate the impact of the cationic lignin polymers in emulsifying oil-water emulsions.
- Expanding scope: Extend the research to encompass emulsions with varying oil types to yield more comprehensive insights.
- Exploring oil-water ratio: Investigate the emulsifier agent's performance by varying the oil-water ratio to assess emulsion stability.
- Complex impeller effects: Future research can delve into the influence of complex impeller configurations on dilute emulsions.
- Droplet size measurement techniques: Compare different techniques for measuring droplet size, including SOPAT, under varying conditions.
- Mixing systems comparison: Compare different mixing systems operating at the same power input, focusing on droplet size distribution using SOPAT.

Nomenclature

Abbreviation

SOPAT	smart online particle analysis technology
DSD	droplet size distribution
OBR	oscillatory baffled reactor
NSERC	natural sciences and engineering research council of Canada
LS	lignosulfonates
IFT	interfacial tension
CFD	computational fluid dynamics
MASM	modified algebraic slip mixture
LBM	lattice-boltzmann method
ORM	optical reflectance measurement
PDPA	phase Doppler particle analyzer
PVM	particle video microscopy
FBRM	focused beam reflectance measurement
KL	kraft lignin
PDADMAC	polydimethyldiallyl ammonium chloride
GPC	gel permeation chromatography
CML	carboxymethylated lignin
HSML	high charge density sulfomethylated lignin
MSML	medium charge density sulfomethylated lignin
LSML	low charge density sulfomethylated lignin
WCA	water contact angle
TSI	turbiscan stability index
H	hydroxyphenyl
G	guaiacyl
S	syringyl
hp	horsepower

Symbols

v_1	volumes (mL) of HCl solution consumed for the first endpoints in blank titration
v_1'	the volumes (mL) of HCl solution consumed for the first endpoints in sample titration
v_2	volumes (mL) of HCl solution consumed for the second endpoints in blank titration
v_2'	the volumes (mL) of HCl solution consumed for the second endpoints in sample titration
v_3	volumes (mL) of HCl solution consumed for the third endpoints in blank titration

v_3'	the volumes (mL) of HCl solution consumed for the third endpoints in sample titration
D_T	diameter of tank (mm)
H_T	height of tank (mm)
H_l	height of inside liquid (mm)
A	oscilation amplitude (mm)
aq	aqueous solution
d_{32}	Sauter mean diameter (μm)
f	oscillation frequency (Hz)
G'	Storage modulus (Pa)
G''	loss modulus (Pa)
hp	Horsepower
n	number of scanning
O/W	oil-in-water emulsion
r	droplet radius (μm)
Rh	Rhodium
W/O	water-in-oil emulsion
x_{bs}	average of x_i
x_i	backscattered light intensity at the scanning time
γ	interfacial tension (mN/m)
ζ	zeta potential (mV)
λ	Wavelength (nm)
ΔP	Laplace pressure (Pa)
φ	oil volume fraction (%)

References

Abdelghafour, M. M., Orbán, Á., Deák, Á., Lamch, Ł., Frank, É., Nagy, R., ... & Janovák, L. (2021). The effect of molecular weight on the solubility properties of biocompatible poly (ethylene succinate) polyester. *Polymers*, *13*(16), 2725.

Abdolmaleki, K., Alizadeh, L., & Nayebzadeh, K. (2019). Temperature dependence of stability, steady and dynamic rheological properties of oil-in-water emulsions stabilized by gum tragacanth. *Journal of Food Measurement and Characterization*, *13*, 1627-1635.

Alinezhad, K., Hosseini, M., Movagarnejad, K., & Salehi, M. (2010). Experimental and modeling approach to study separation of water in crude oil emulsion under non-uniform electrical field. *Korean Journal of Chemical Engineering*, *27*, 198-205.

Alopaeus, V., Koskinen, J., Keskinen, K. I., & Majander, J. (2002). Simulation of the population balances for liquid–liquid systems in a nonideal stirred tank. Part 2—parameter fitting and the use of the multiblock model for dense dispersions. *Chemical Engineering Science*, *57*(10), 1815-1825.

Alwadani, N., & Fatehi, P. (2018). Synthetic and lignin-based surfactants: Challenges and opportunities. *Carbon Resources Conversion*, *1*(2), 126-138.

Anderson, P. D., & Meijer, H. E. (2009). Scale-down of mixing equipment: microfluidics. *Mixing and Compounding of Polymers: Theory and Practice*, 645-699.

Ataie, M., Sutherland, K., Pakzad, L., & Fatehi, P. (2020). Experimental and modeling analysis of lignin derived polymer in flocculating aluminium oxide particles. *Separation and Purification Technology*, *247*, 116944.

Avila, M., Kawas, B., Fletcher, D. F., Poux, M., Xuereb, C., & Aubin, J. (2022). Design, performance characterization and applications of continuous oscillatory baffled reactors. *Chemical Engineering and Processing-Process Intensification*, *180*, 108718.

Awasthi, M. K., Sarsaiya, S., Patel, A., Juneja, A., Singh, R. P., Yan, B., ... & Taherzadeh, M. J. (2020). Refining biomass residues for sustainable energy and bio-products: An assessment of technology, its importance, and strategic applications in circular bio-economy. *Renewable and Sustainable Energy Reviews*, *127*, 109876.

Bahrpaima, K., & Fatehi, P. (2018). Synthesis and characterization of carboxyethylated lignosulfonate. *ChemSusChem*, *11*(17), 2967-2980.

Binks, B. P., Dong, J., & Rebolj, N. (1999). Equilibrium phase behaviour and emulsion stability in silicone oil+ water+ AOT mixtures. *Physical Chemistry Chemical Physics*, *1*(9), 2335-2344.

Blais, B., & Bertrand, F. (2017). CFD-DEM investigation of viscous solid–liquid mixing: Impact of particle properties and mixer characteristics. *Chemical Engineering Research and Design*, *118*, 270-285.

Blais, B., Bertrand, O., Fradette, L., & Bertrand, F. (2017). CFD-DEM simulations of early turbulent solid–liquid mixing: Prediction of suspension curve and just-suspended speed. *Chemical Engineering Research and Design*, *123*, 388-406.

Blais, B., Lassaigne, M., Goniva, C., Fradette, L., & Bertrand, F. (2016). Development of an unresolved CFD–DEM model for the flow of viscous suspensions and its application to solid–liquid mixing. *Journal of Computational Physics*, *318*, 201-221.

Boerjan, W., Ralph, J., & Baucher, M. (2003). Lignin biosynthesis. *Annual Review of Plant Biology*, *54*(1), 519-546.

Bonto, M., Eftekhari, A. A., & Nick, H. M. (2019). An overview of the oil-brine interfacial behavior and a new surface complexation model. *Scientific Reports*, *9*(1), 6072.

Boxall, J. A., Koh, C. A., Sloan, E. D., Sum, A. K., & Wu, D. T. (2010). Measurement and calibration of droplet size distributions in water-in-oil emulsions by particle video microscope and a focused beam reflectance method. *Industrial & Engineering Chemistry Research*, *49*(3), 1412-1418.

Canu, R., Puggelli, S., Essadki, M., Duret, B., Menard, T., Massot, M., ... & Demoulin, F. X. (2018). Where does the droplet size distribution come from?. *International Journal of Multiphase Flow*, *107*, 230-245.

Carrillo, C. A., Saloni, D., Lucia, L. A., Hubbe, M. A., & Rojas, O. J. (2012). Capillary flooding of wood with microemulsions from Winsor I systems. *Journal of Colloid and Interface Science*, *381*(1), 171-179.

Celia, C., Trapasso, E., Cosco, D., Paolino, D., & Fresta, M. (2009). Turbiscan Lab® Expert analysis of the stability of ethosomes® and ultradeformable liposomes containing a bilayer fluidizing agent. *Colloids and Surfaces B: Biointerfaces*, *72*(1), 155-160.

Chakar, F. S., & Ragauskas, A. J. (2004). Review of current and future softwood kraft lignin process chemistry. *Industrial Crops and Products*, *20*(2), 131-141.

Chakar, F. S., & Ragauskas, A. J. (2004). Review of current and future softwood kraft lignin process chemistry. *Industrial crops and products*, *20*(2), 131-141.Chang, C. C., Letteri, R., Hayward, R. C., & Emrick, T. (2015). Functional sulfobetaine polymers: synthesis and salt-responsive stabilization of oil-in-water droplets. *Macromolecules*, *48*(21), 7843-7850.

Chappat, M. (1994). Some applications of emulsions. *Colloids and Surfaces A: Physicochemical and Engineering Aspects*, *91*, 57-77.

Chen, C., Zhu, M., Li, M., Fan, Y., & Sun, R. C. (2016). Epoxidation and etherification of alkaline lignin to prepare water-soluble derivatives and its performance in improvement of enzymatic hydrolysis efficiency. *Biotechnology for Biofuels*, *9*(1), 1-15.

Chen, Y., Zhang, H., Zhu, Z., & Fu, S. (2020). High-value utilization of hydroxymethylated lignin in polyurethane adhesives. *International Journal of Biological Macromolecules*, *152*, 775-785.

Cortés-Triviño, E., Valencia, C., Delgado, M. A., & Franco, J. M. (2018). Modification of alkali lignin with poly (ethylene glycol) diglycidyl ether to be used as a thickener in bio-lubricant formulations. *Polymers*, *10*(6), 670.

Costa, C., Medronho, B., Filipe, A., Mira, I., Lindman, B., Edlund, H., & Norgren, M. (2019). Emulsion formation and stabilization by biomolecules: The leading role of cellulose. *Polymers*, *11*(10), 1570.

Crepaldi, E. L., Pavan, P. C., Tronto, J., & Valim, J. B. (2002). Chemical, structural, and thermal properties of Zn (II)–Cr (III) layered double hydroxides intercalated with sulfated and sulfonated surfactants. *Journal of Colloid and Interface Science*, *248*(2), 429-442.

Derkacheva, O., & Sukhov, D. (2008, May). Investigation of lignins by FTIR spectroscopy. In *Macromolecular symposia* (Vol. 265, No. 1, pp. 61-68). Weinheim: WILEY-VCH Verlag.

Dessbesell, L., Paleologou, M., Leitch, M., Pulkki, R., & Xu, C. C. (2020). Global lignin supply overview and kraft lignin potential as an alternative for petroleum-based polymers. *Renewable and Sustainable Energy Reviews*, *123*, 109768.

Dowding, P. J., Goodwin, J. W., & Vincent, B. (2001). Factors governing emulsion droplet and solid particle size measurements performed using the focused beam reflectance technique. *Colloids and surfaces A: Physicochemical and Engineering Aspects*, *192*(1-3), 5-13.

Duan, X., Feng, X., Peng, C., Yang, C., & Mao, Z. (2020). Numerical simulation of micro-mixing in gas–liquid and solid–liquid stirred tanks with the coupled CFD-E-model. *Chinese Journal of Chemical Engineering*, *28*(9), 2235-2247.

El-Hamouz, A., Cooke, M., Kowalski, A., & Sharratt, P. (2009). Dispersion of silicone oil in water surfactant solution: Effect of impeller speed, oil viscosity and addition point on drop size distribution. *Chemical Engineering and Processing*, *48*(2), 633-642.

Espinoza-Acosta, J. L., Torres-Chávez, P. I., Ramírez-Wong, B., López-Saiz, C. M., & Montaño-Leyva, B. (2016). Antioxidant, antimicrobial, and antimutagenic properties of technical lignins and their applications. *BioResources*, *11*(2), 5452-5481.

Falco, J. W., Walker Jr, R. D., & Shah, D. O. (1974). Effect of phase-volume ratio and phase-inversion on viscosity of microemulsions and liquid crystals. *AIChE Journal*, *20*(3), 510-514.

Fatehi, P., & Chen, J. (2016). Extraction of technical lignins from pulping spent liquors, challenges and opportunities. *Production of Biofuels and Chemicals from Lignin*, 35-54.

Fengel, D., & Wegener, G. (Eds.). (2011). *Wood: Chemistry, Ultrastructure, Reactions*. Walter de Gruyter.

Fingas, M., & Fieldhouse, B. (2004). Formation of water-in-oil emulsions and application to oil spill modelling. *Journal of Hazardous Materials*, *107*(1-2), 37-50.

Floury, J., Desrumaux, A., & Lardières, J. (2000). Effect of high-pressure homogenization on droplet size distributions and rheological properties of model oil-in-water emulsions. *Innovative Food Science & Emerging Technologies*, *1*(2), 127-134.

Fragkopoulos, A. A., Pairam, E., Berger, E., Segre, P. N., & Fernández-Nieves, A. (2017). Shrinking instability of toroidal droplets. *Proceedings of the National Academy of Sciences*, *114*(11), 2871-2875.

Gao, W., Inwood, J. P., & Fatehi, P. (2019). Sulfonation of phenolated kraft lignin to produce water soluble products. *Journal of Wood Chemistry and Technology*, 39(4), 225-241.

Gellerstedt, G., & Gustafsson, K. (1987). Structural changes in lignin during kraft cooking. Part 5. Analysis of dissolved lignin by oxidative degradation. *Journal of Wood Chemistry and Technology*, *7*(1), 65-80.

Ghaemi, A., Hübner, M., Minceva, M., & Germann, N. (2021). Phase field analysis of binary mixtures with partially miscible components. *International Journal of Multiphase Flow*, *138*, 103613.

Ghaffar, S. H., & Fan, M. (2013). Structural analysis for lignin characteristics in biomass straw. *Biomass and Bioenergy*, *57*, 264-279.

Ghannam, M. T., Hasan, S. W., Abu-Jdayil, B., & Esmail, N. (2012). Rheological properties of heavy & light crude oil mixtures for improving flowability. *Journal of Petroleum Science and Engineering*, *81*, 122-128.

Gharehkhani, S., Ghavidel, N., & Fatehi, P. (2018). Kraft lignin–tannic acid as a green stabilizer for oil/water emulsion. *ACS Sustainable Chemistry & Engineering*, *7*(2), 2370-2379.

Gharehkhani, S., Zhang, Y., & Fatehi, P. (2019). Lignin-derived platform molecules through TEMPO catalytic oxidation strategies. *Progress in Energy and Combustion Science*, *72*, 59-89.

Ghavidel, N., & Fatehi, P. (2020). Pickering/Non-Pickering Emulsions of Nanostructured Sulfonated Lignin Derivatives. *ChemSusChem*, *13*(17), 4567-4578.

Ghosh, S., & Rousseau, D. (2010). Emulsion breakdown in foods and beverages. In *Chemical deterioration and physical instability of food and beverages* (pp. 260-295). Woodhead Publishing.

Ghotli, R. A., Abbasi, M. R., Bagheri, A., Raman, A. A. A., Ibrahim, S., & Bostanci, H. (2019). Experimental and modeling evaluation of droplet size in immiscible liquid-liquid stirred vessel using various impeller designs. *Journal of the Taiwan Institute of Chemical Engineers*, *100*, 26-36.

Giapos, A., Pachatouridis, C., & Stamatoudis, M. (2005). Effect of the number of impeller blades on the drop sizes in agitated dispersions. *Chemical Engineering Research and Design*, *83*(12), 1425-1430.

Gillet, S., Aguedo, M., Petitjean, L., Morais, A. R. C., da Costa Lopes, A. M., Łukasik, R. M., & Anastas, P. T. (2017). Lignin transformations for high value applications: towards targeted modifications using green chemistry. *Green Chemistry*, *19*(18), 4200-4233.

Godfrey, J.C.; Grilc, V. (Eds.) Drop Size and Drop Size Distributions for Liquid-Liquid Dispersions in Agitated Tanks of Square Cross Section. In Proceedings of the 2nd European Conference on Mixing, Cambridge, UK, 22–27 June 1977; BHRA Fluid Engineering: Cambridge, UK, 1977; pp. 1–20.Goodarzi, F., & Zendehboudi, S. (2019). A comprehensive review on emulsions and emulsion stability in chemical and energy industries. *The Canadian Journal of Chemical Engineering*, *97*(1), 281-309.

Gréa, B. J., Griffond, J., & Burlot, A. (2014). The effects of variable viscosity on the decay of homogeneous isotropic turbulence. *Physics of Fluids*, *26*(3).

Gu, D., Mei, Y., Wen, L., Wang, X., & Liu, Z. (2021). Chaotic mixing and mass transfer characteristics of fractal impellers in gas-liquid stirred tank. *Journal of the Taiwan Institute of Chemical Engineers*, *121*, 20-28.

Has, C., & Sunthar, P. (2021). Colloidal fingering in miscible liquids. *Colloid and Interface Science Communications*, *41*, 100368.

He, W., & Fatehi, P. (2015). Preparation of sulfomethylated softwood kraft lignin as a dispersant for cement admixture. *Royal Society of Chemistry Advances*, *5*(58), 47031-47039.

Healy, R. N., Reed, R. L., & Stenmark, D. G. (1976). Multiphase microemulsion systems. *Society of Petroleum Engineers Journal*, *16*(03), 147-160.

Heidari, A. (2020). CFD simulation of impeller shape effect on quality of mixing in two-phase gas–liquid agitated vessel. *Chinese Journal of Chemical Engineering*, *28*(11), 2733-2745.

Hiraoka, S., Kato, Y., Tada, Y., Ozaki, N., Murakami, Y., & Lee, Y. S. (2001). Power consumption and mixing time in an agitated vessel with double impeller. *Chemical Engineering Research and Design*, *79*(8), 805-810.

Hohl, L., J.M. Schulz, and M. Kraume, *Towards Drop Size Modeling in Three Phase Microemulsion Systems. Journal of Chemical Engineering of Japan*, 2018. **51**(4): p. 383-388.

Hole, L. R., Dagestad, K. F., Röhrs, J., Wettre, C., Kourafalou, V. H., Androulidakis, Y., ... & Garcia-Pineda, O. (2019). The DeepWater Horizon oil slick: simulations of river front effects and oil droplet size distribution. *Journal of Marine Science and Engineering*, *7*(10), 329.

Hu, M., & Russell, T. P. (2021). Polymers with advanced architectures as emulsifiers for multi-functional emulsions. *Materials Chemistry Frontiers*, *5*(3), 1205-1220.

Ibrahim, S., Choong, C. E., & El-Shafie, A. (2019). Sensitivity analysis of artificial neural networks for just-suspension speed prediction in solid-liquid mixing systems: Performance comparison of MLPNN and RBFNN. *Advanced Engineering Informatics*, 39, 278-291.

Jahan, M. S., Liu, Z., Wang, H., Saeed, A., & Ni, Y. (2012). Isolation and characterization of lignin from prehydrolysis liquor of kraft-based dissolving pulp production. Cellulose Chemistry and Technology, 46(3-4), 261-267.

Jiao, G. J., Xu, Q., Cao, S. L., Peng, P., & She, D. (2018). Controlled-release fertilizer with lignin used to trap urea/hydroxymethylurea/urea-formaldehyde polymers. *BioResources*, *13*(1), 1711-1728.

Jiao, Y., Zhao, Y., Chang, Y., Ma, Z., Kobayashi, I., Nakajima, M., & Neves, M. A. (2022). Enhancing the Formation and Stability of Oil-In-Water Emulsions Prepared by Microchannels Using Mixed Protein Emulsifiers. *Frontiers in Nutrition*, *9*, 822053.

Kai, D., Tan, M. J., Chee, P. L., Chua, Y. K., Yap, Y. L., & Loh, X. J. (2016). Towards lignin-based functional materials in a sustainable world. *Green Chemistry*, *18*(5), 1175-1200.

Kalami, S., Chen, N., Borazjani, H., & Nejad, M. (2018). Comparative analysis of different lignins as phenol replacement in phenolic adhesive formulations. *Industrial Crops and Products*, *125*, 520-528.

Kalliola, S., Repo, E., Srivastava, V., Zhao, F., Heiskanen, J. P., Sirviö, J. A., ... & Sillanpää, M. (2018). Carboxymethyl chitosan and its hydrophobically modified derivative as pH-switchable emulsifiers. *Langmuir*, *34*(8), 2800-2806.

Kazzaz, A. E., & Fatehi, P. (2020). Technical lignin and its potential modification routes: A mini-review. *Industrial Crops and Products*, *154*, 112732.

Khan, B. A., Akhtar, N., Khan, H. M. S., Waseem, K., Mahmood, T., Rasul, A., ... & Khan, H. (2011). Basics of pharmaceutical emulsions: A review. *African Journal of Pharmacy and Pharmacology*, *5*(25), 2715-2725.

Kim, H., Lee, J., Kim, T. H., & Kim, H. Y. (2015). Spontaneous marangoni mixing of miscible liquids at a liquid–liquid–air contact line. *Langmuir*, 31(31), 8726-8731.

Kim, Y. J., Liu, Y. D., Seo, Y., & Choi, H. J. (2013). Pickering-emulsion-polymerized polystyrene/Fe2O3 composite particles and their magnetoresponsive characteristics. *Langmuir*, *29*(16), 4959-4965.

Konduri, M. K., & Fatehi, P. (2015). Production of water-soluble hardwood kraft lignin via sulfomethylation using formaldehyde and sodium sulfite. *ACS Sustainable Chemistry & Engineering*, *3*(6), 1172-1182.

Konduri, M. K., Kong, F., & Fatehi, P. (2015). Production of carboxymethylated lignin and its application as a dispersant. *European Polymer Journal. 70*, 371-383.

Kong, F., Wang, S., Price, J. T., Konduri, M. K., & Fatehi, P. (2015). Water soluble kraft lignin–acrylic acid copolymer: Synthesis and characterization. *Green Chemistry*, *17*(8), 4355-4366.

Kouisni, L., Holt-Hindle, P., Maki, K., & Paleologou, M. (2012). The lignoforce system: a new process for the production of high-quality lignin from black liquor. *Journal of Science & Technology for Forest Products and Processes*, *2*(4), 6-10.

Kowalska, M., Krztoń-Maziopa, A., Babut, M., & Mitrosz, P. (2020). Rheological and physical analysis of oil-water emulsion based on enzymatic structured fat. *Rheologica Acta*, *59*, 717-726.

Kühnel, I., Saake, B., & Lehnen, R. (2018). A New Environmentally Friendly Approach to Lignin-Based Cyclic Carbonates. *Macromolecular Chemistry and Physics*, *219*(7), 1700613.

Kumar, S., Kumar, R., & Gandhi, K. S. (1991). Alternative mechanisms of drop breakage in stirred vessels. *Chemical Engineering Science*, *46*(10), 2483-2489.

Laurichesse, S., & Avérous, L. (2014). Chemical modification of lignins: Towards biobased polymers. *Progress in Polymer Science*, *39*(7), 1266-1290.

Leng, D. E., & Calabrese, R. V. (2003). Immiscible liquid–liquid systems. *Handbook of Industrial Mixing: Science and Practice*, 639-753.

Li, C., Zhao, X., Wang, A., Huber, G. W., & Zhang, T. (2015). Catalytic transformation of lignin for the production of chemicals and fuels. *Chemical Reviews*, *115*(21), 11559-11624.

Li, S., Willoughby, J. A., & Rojas, O. J. (2016). Oil-in-Water Emulsions Stabilized by Carboxymethylated Lignins: Properties and Energy Prospects. *ChemSusChem*, *9*(17), 2460-2469.

Li, Y., & Yang, L. (2015). Driving forces for drug loading in drug carriers. *Journal of Microencapsulation*, *32*(3), 255-272.

Liu, N., Wang, W., Tian, Y., Wu, C., & Gong, J. (2017). Experimental and numerical study for drop size distribution in oil-water dispersions with nonionic surfactant Tween 80. *Experimental Thermal and Fluid Science*, *89*, 153-165.

Liu, Y., Daum, P. H., & Yum, S. S. (2006). Analytical expression for the relative dispersion of the cloud droplet size distribution. *Geophysical Research Letters*, *33*(2).

Lobry, E., Lasuye, T., Gourdon, C., & Xuereb, C. (2015). Liquid–liquid dispersion in a continuous oscillatory baffled reactor–Application to suspension polymerization. *Chemical Engineering Journal*, *259*, 505-518.

Lovick, J., Mouza, A. A., Paras, S. V., Lye, G. J., & Angeli, P. (2005). Drop size distribution in highly concentrated liquid–liquid dispersions using a light back scattering method. *Journal of Chemical Technology & Biotechnology: International Research in Process, Environmental & Clean Technology*, *80*(5), 545-552.

Maaß, S., Rojahn, J., Hänsch, R., & Kraume, M. (2012). Automated drop detection using image analysis for online particle size monitoring in multiphase systems. *Computers & Chemical Engineering*, *45*, 27-37.

Macfarlane, A. L., Mai, M., & Kadla, J. F. (2014). Bio-based chemicals from biorefining: Lignin conversion and utilisation. In *Advances in Biorefineries* (pp. 659-692). Woodhead Publishing.

Madhania, S., Nurtono, T., Cahyani, A. B., Muharam, Y., Winardi, S., & Purwanto, W. W. (2017). Mixing behaviour of miscible liquid-liquid multiphase flow in stirred tank with different marine propeller installment by computational fluid dynamics method. *Chemical Engineering Transactions*, *56*, 1057-1062.

Madzhidova, V. E., Dalimova, G. N., & Abduazimov, K. A. (1998). Sulfomethylation of lignins. *Chemistry of Natural Compounds*, *34*, 179-181.

Maindarkar, S. N., Hoogland, H., & Henson, M. A. (2015). Predicting the combined effects of oil and surfactant concentrations on the drop size distributions of homogenized emulsions. *Colloids and Surfaces A: Physicochemical and Engineering Aspects*, *467*, 18-30.

Maphosa, Y., & Jideani, V. A. (2018). Factors affecting the stability of emulsions stabilised by biopolymers. *Science and technology behind Nanoemulsions*, *65*.

Mathias, A. L., & Rodrigues, A. E. (1995). Production of vanillin by oxidation of pine kraft lignins with oxygen.

McClements, D. J., Decker, E. A., & Weiss, D. J. (2007). Emulsion-based delivery systems for lipophilic bioactive components. *Journal of Food Science*, *72*(8), R109-R124.

McDonald, A. G., & Donaldson, L. A. (2001). Constituents in wood. *Encyclopedia of Materials: Science and Technology. Elsevier Science*, 9612-9616.

McLean, J. D., & Kilpatrick, P. K. (1997). Effects of asphaltene solvency on stability of water-in-crude-oil emulsions. *Journal of Colloid and Interface Science*, *189*(2), 242-253.

Mohammed, R. A., Bailey, A. I., Luckham, P. F., & Taylor, S. E. (1994). The effect of demulsifiers on the interfacial rheology and emulsion stability of water-in-crude oil emulsions. *Colloids and Surfaces A: Physicochemical and Engineering Aspects*, *91*, 129-139.

Mollakhalili Meybodi, N., Mohammadifar, M. A., & Abdolmaleki, K. H. (2014). Effect of dispersed phase volume fraction on physical stability of oil-in-water emulsion in the presence of gum tragacanth. *Journal of Food Quality and Hazards Control*, *1*(4), 102-107.

Moradi, M., Alvarado, V., & Huzurbazar, S. (2011). Effect of salinity on water-in-crude oil emulsion: evaluation through drop-size distribution proxy. *Energy & Fuels*, *25*(1), 260-268.

Naeeni, S. K., & Pakzad, L. (2019). Experimental and numerical investigation on mixing of dilute oil in water dispersions in a stirred tank. *Chemical Engineering Research and Design*, *147*, 493-509.

Nagata, S. (1975). Agitation in Gas–Liquid Systems. *Mixing: Principles and Applications," Halsted Press, Shinji Nagata*, 458.

Ni, X., Zhang, Y., & Mustafa, I. (1998). An investigation of droplet size and size distribution in methylmethacrylate suspensions in a batch oscillatory-baffled reactor. *Chemical Engineering Science*, *53*(16), 2903-2919.

O'Rourke, A. M., & MacLoughlin, P. F. (2005). A comparison of measurement techniques used in the analysis of evolving liquid–liquid dispersions. *Chemical Engineering and Processing: Process Intensification*, *44*(8), 885-894.

Österberg, M., Sipponen, M. H., Mattos, B. D., & Rojas, O. J. (2020). Spherical lignin particles: A review on their sustainability and applications. *Green Chemistry*, *22*(9), 2712-2733.

P. Bajpai, Biermann's Handbook of Pulp and Paper: Raw Material and Pulp Making, Elsevier 2018.

Pacek, A. W., Chamsart, S., Nienow, A. W., & Bakker, A. (1999). The influence of impeller type on mean drop size and drop size distribution in an agitated vessel. *Chemical Engineering Science*, *54*(19), 4211-4222.

Panckow, R. P., Comandè, G., Maaß, S., & Kraume, M. (2015). Determination of particle size distributions in multiphase systems containing nonspherical fluid particles. *Chemical Engineering & Technology*, *38*(11), 2011-2016.

Panckow, R. P., Reinecke, L., Cuellar, M. C., & Maaß, S. (2017). Photo-optical in-situ measurement of drop size distributions: Applications in research and industry. *Oil & Gas Science and Technology–Revue d'IFP Energies nouvelles*, *72*(3), 14.

Partal. P., Guerrero, A., Berjano, M., & Gallegos, C. (1997). Influence of concentration and temperature on the flow behavior of oil-in-water emulsions stabilized by sucrose palmitate. *Journal of the American Oil Chemists' Society*, *74*(10), 1203-1212.

Pereira, N. E. (2002). *Characterisation of a continuous oscillatory baffled tubular reactor* (Doctoral dissertation, Heriot-Watt University).

Perlekar, P., Biferale, L., Sbragaglia, M., Srivastava, S., & Toschi, F. (2012). Droplet size distribution in homogeneous isotropic turbulence. *Physics of Fluids*, *24*(6).

Podkościelna, B., Sobiesiak, M., Zhao, Y., Gawdzik, B., & Sevastyanova, O. (2015). Preparation of lignin-containing porous microspheres through the copolymerization of lignin acrylate derivatives with styrene and divinylbenzene. *Holzforschung*, *69*(6), 769-776.

Quadros, P. A., & Baptista, C. M. (2003). Effective interfacial area in agitated liquid–liquid continuous reactors. *Chemical Engineering Science*, *58*(17), 3935-3945.

Raja Ehsan Shah, R. S. S., Sajjadi, B., Abdul Raman, A. A., & Ibrahim, S. (2015). Solid-liquid mixing analysis in stirred vessels. Reviews in Chemical Engineering, 31(2), 119-147.

Ralph, J., Lundquist, K., Brunow, G., Lu, F., Kim, H., Schatz, P. F., ... & Boerjan, W. (2004). Lignins: natural polymers from oxidative coupling of 4-hydroxyphenyl-propanoids. *Phytochemistry Reviews*, *3*, 29-60.

Raya, S. A., Mohd Saaid, I., Abbas Ahmed, A., & Abubakar Umar, A. (2020). A critical review of development and demulsification mechanisms of crude oil emulsion in the petroleum industry. *Journal of Petroleum Exploration and Production Technology*, *10*, 1711-1728.

Rodrigues, A. E., Pinto, P. C. D. O. R., Barreiro, M. F., Esteves da Costa, C. A., Ferreira da Mota, M. I., Fernandes, I., ... & Fernandes, I. (2018). Chemical pulp mills as biorefineries. *An Integrated Approach for Added-Value Products from Lignocellulosic Biorefineries: Vanillin, Syringaldehyde, Polyphenols and Polyurethane*, 1-51.

Röhl, S., Hohl, L., Kempin, M., Enders, F., Jurtz, N., & Kraume, M. (2019). Influence of different silica nanoparticles on drop size distributions in agitated liquid-liquid systems. *Chemie Ingenieur Technik*, *91*(11), 1640-1655.

Rojo, E., Peresin, M. S., Sampson, W. W., Hoeger, I. C., Vartiainen, J., Laine, J., & Rojas, O. J. (2015). Comprehensive elucidation of the effect of residual lignin on the physical. barrier, mechanical and surface properties of nanocellulose films. *Green Chemistry*, *17*(3), 1853-1866.

Rossi, A., Alberini, F., & Brunazzi, E. (2022). Identification of suspension state using passive acoustic emission and machine learning in a solid–liquid mixing system. *Chemical Engineering Research and Design*, *177*, 273-282.

Rosti, M. E., & Takagi, S. (2021). Shear-thinning and shear-thickening emulsions in shear flows. *Physics of Fluids*, *33*(8).

Sahasrabudhe, S. N., Rodriguez-Martinez, V., O'Meara, M., & Farkas, B. E. (2017). Density, viscosity, and surface tension of five vegetable oils at elevated temperatures: Measurement and modeling. International Journal of Food Properties, 20(sup2), 1965-1981.

Schramm, L. L., Stasiuk, E. N., & Marangoni, D. G. (2003). 2 Surfactants and their applications. *Annual Reports Section" C"(Physical Chemistry)*, *99*, 3-48.

Sengupta, B., Sengupta, R., & Subrahmanyam, N. (2006). Process intensification of copper extraction using emulsion liquid membranes: Experimental search for optimal conditions. *Hydrometallurgy*, *84*(1-2), 43-53.

Sequeiros, A., Serrano, L., & Labidi, J. (2016). Bromination of guaiacol and syringol using ionic liquids to obtain bromides. *Journal of Chemical Technology & Biotechnology*, *91*(6), 1809-1815.

Solsvik, J., & Jakobsen, H. A. (2015). Single drop breakup experiments in stirred liquid–liquid tank. *Chemical Engineering Science*, *131*, 219-234.

Spicer, P. T., Keller, W., & Pratsinis, S. E. (1996). The effect of impeller type on floc size and structure during shear-induced flocculation. *Journal of Colloid and Interface Science*, *184*(1), 112-122.

Stamatoudis, M., & Tavlarides, L. L. (1987). The effect of continuous-phase viscosity on the unsteady state behavior of liquid-liquid agitated dispersions. *The Chemical Engineering Journal. 35*(2), 137-143.

Sun, R. (2010). *Cereal straw as a resource for sustainable biomaterials and biofuels: chemistry, extractives, lignins, hemicelluloses and cellulose*. Elsevier.

Sun, Z., Fridrich, B., De Santi, A., Elangovan, S., & Barta, K. (2018). Bright side of lignin depolymerization: toward new platform chemicals. *Chemical Reviews*, *118*(2), 614-678.

Tadros, T. F. (2013). Emulsion formation, stability, and rheology. *Emulsion Formation and Stability*, 1-75.

Taherian, A. R., Fustier, P., & Ramaswamy, H. S. (2006). Effect of added oil and modified starch on rheological properties, droplet size distribution, opacity and stability of beverage cloud emulsions. *Journal of Food Engineering*, *77*(3), 687-696.

Tambe, D. E., & Sharma, M. M. (1995). Factors controlling the stability of colloid-stabilized emulsions: III. Measurement of the rheological properties of colloid-laden interfaces. *Journal of Colloid and Interface Science*, *171*(2), 456-462.

Tan, C., & McClements, D. J. (2021). Application of advanced emulsion technology in the food industry: A review and critical evaluation. *Foods*, *10*(4), 812.

Tang, Q., Zhang, J., Wu, Y., Wang, Y., & Liu, Z. (2020). An experimental study of immiscible liquid–liquid dispersions in a pump–mixer of mixer–settler. *Chinese Journal of Chemical Engineering*, *28*(1), 33-45.

Tarasov, D., Leitch, M., & Fatehi, P. (2018). Lignin–carbohydrate complexes: properties, applications, analyses, and methods of extraction: a review. *Biotechnology for Biofuels*, *11*(1), 1-28.

Tcholakova, S., Lesov, I., Golemanov, K., Denkov, N. D., Judat, S., Engel, R., & Danner, T. (2011). Efficient emulsification of viscous oils at high drop volume fraction. *Langmuir*, *27*(24), 14783-14796.

Tian, J., Ren, S., Fang, G., Ma, Y., & Ai, Q. (2014). Preparation and performance of dimethyl-acetoxy-(2-carboxymethylether)-lignin ammonium chloride amphoteric surfactant. *BioResources*, *9*(4), 6290-6303.

Upton, B. M., & Kasko, A. M. (2016). Strategies for the conversion of lignin to high-value polymeric materials: review and perspective. *Chemical Reviews*, *116*(4), 2275-2306.

Urbina-Villalba, G. (2009). An algorithm for emulsion stability simulations: Account of flocculation, coalescence, surfactant adsorption and the process of Ostwald ripening. *International Journal of Molecular Sciences*, *10*(3), 761-804.

Van Heiningen, A. (2006). Converting a kraft pulp mill into an integrated forest biorefinery. *Pulp and Paper Canada*, *107*(6), 38-43.

Venkataramani, D., Tsulaia, A., & Amin, S. (2020). Fundamentals and applications of particle stabilized emulsions in cosmetic formulations. *Advances in Colloid and Interface Science*, *283*, 102234.

Verhoff, F. H., Ross, S. L., & Curl, R. L. (1977). Breakage and coalescence processes in an agitated dispersion. Experimental system and data reduction. *Industrial & Engineering Chemistry Fundamentals*, *16*(3), 371-377.

Wade, J. B., Martin, G. P., & Long, D. F. (2014). Feasibility assessment for a novel reverse-phase wet granulation process: The effect of liquid saturation and binder liquid viscosity. *International Journal of Pharmaceutics*, *475*(1-2), 450-461.

Wang, W., Liu, J., Wang, P., Duan, J., & Gong, J. (2013). Evolution of dispersed drops during the mixing of mineral oil and water phases in a stirringtank. *Chemical Engineering Science*, *91*, 173-179.

Wang, W., Zhao, S., Shao, T., Jin, Y., & Cheng, Y. (2012). Visualization of micro-scale mixing in miscible liquids using μ-LIF technique and drug nano-particle preparation in T-shaped micro-channels. *Chemical Engineering Journal*, *192*, 252-261.

Wu J., Ma G., Recent Studies of Pickering Emulsions: Particles Make the Difference, Small Weinheim an der Bergstrasse, Germany, 2016, 12(34), 4633–48.

Xiao, J., Gonzalez, A. J. P., & Huang, Q. (2016). Kafirin nanoparticles-stabilized Pickering emulsions: Microstructure and rheological behavior. *Food Hydrocolloids*, *54*, 30-39.

Xie, R., & Vorobev, A. (2016). On the phase-field modelling of a miscible liquid/liquid boundary. *Journal of Colloid and Interface Science*, *464*, 48-58.

Yang, W., Fortunati, E., Gao, D., Balestra, G. M., Giovanale, G., He, X., ... & Puglia, D. (2018). Valorization of acid isolated high yield lignin nanoparticles as innovative antioxidant/antimicrobial organic materials. *ACS Sustainable Chemistry & Engineering*, *6*(3), 3502-3514.

Zainal Abidin, M. I. I., Abdul Raman, A. A., & Mohamad Nor, M. I. (2014). Experimental investigations in liquid–liquid dispersion system: effects of dispersed phase viscosity and impeller speed. *Industrial & Engineering Chemistry Research*, *53*(15), 6554-6561.

Zakzeski, J., Bruijnincx, P. C., Jongerius, A. L., & Weckhuysen, B. M. (2010). The catalytic valorization of lignin for the production of renewable chemicals. *Chemical Reviews*, *110*(6), 3552-3599.

Zembyla, M., Murray, B. S., & Sarkar, A. (2020). Water-in-oil emulsions stabilized by surfactants, biopolymers and/or particles: A review. *Trends in Food Science & Technology*, *104*, 49-59.

Zeng, L., Zhang, Y., Bukirwa, C., Li, W., & Yang, Y. (2015). Study of mean diameter and drop size distribution of emulsion drops in a modified rotating disc contactor for an emulsion liquid membrane system. *RSC advances*, *5*(109), 89959-89970.

Zha, R., Shi, T., Zhang, Z., Xu, D., Jiang, T., & Zhang, M. (2017). Quasi-reverse-emulsion-templated approach for a facile and sustainable environmental remediation for cadmium. *RSC Advances*, *7*(11), 6345-6357.

Zhang, B., Yang, D., Wang, H., Qian, Y., Huang, J., Yu, L., & Qiu, X. (2018). Activation of enzymatic hydrolysis lignin by NaOH/urea aqueous solution for enhancing its sulfomethylation reactivity. *ACS Sustainable Chemistry & Engineering*, *7*(1), 1120-1128.

Zhang, H., Bai, Y., Zhou, W., & Chen, F. (2017). Color reduction of sulfonated eucalyptus kraft lignin. *International journal of biological macromolecules*, *97*, 201-208.

Zhang, J., Xu, S., & Li, W. (2012). High shear mixers: A review of typical applications and studies on power draw, flow pattern, energy dissipation and transfer properties. *Chemical Engineering and Processing: Process Intensification*, *57*, 25-41.

Zhang, Y., Guo, S., Ren, X., Liu, X., & Fang, Y. (2017). CO2 and redox dual responsive Pickering emulsion. *Langmuir*, *33*(45), 12973-12981.

Zhao, Y., Li, X., Cheng, J., Yang, C., & Mao, Z. S. (2011). Experimental study on liquid–liquid macromixing in a stirred tank. *Industrial & Engineering Chemistry Research*, *50*(10), 5952-5958.

Zheng, Q., Chai, L., Du, B., Li, W., Fu, L. H., & Chen, X. (2023). A pH-Sensitive Lignin-Based Material for Sustained Release of 8-Hydroxyquinoline. *Polymers*, *15*(8), 1867.

Zheng, T., Zheng, D., Li, X., Cai, C., Lou, H., Liu, W., & Qiu, X. (2017). Synthesis of quaternized lignin and its clay-tolerance properties in montmorillonite-containing cement paste. *ACS Sustainable Chemistry & Engineering*, *5*(9), 7743-7750.

Zhou, G., & Kresta, S. M. (1996). Impact of tank geometry on the maximum turbulence energy dissipation rate for impellers. *AIChE Journal. 42*(9), 2476-2490.

Zhou, G., & Kresta, S. M. (1998). Correlation of mean drop size and minimum drop size with the turbulence energy dissipation and the flow in an agitated tank. *Chemical Engineering Science*, *53*(11), 2063-2079.

Zhou, G., & Kresta, S. M. (1998). Evolution of drop size distribution in liquid–liquid dispersions for various impellers. *Chemical Engineering Science*, *53*(11), 2099-2113.

Zhou, Y., Yin, D., Chen, W., Liu, B., & Zhang, X. (2019). A comprehensive review of emulsion and its field application for enhanced oil recovery. *Energy Science & Engineering*, *7*(4), 1046-1058.